

Natural Product-Based 1,2,3-Triazole/Sulfonate Analogues as Potential Chemotherapeutic Agents for Bacterial Infections

Babita Aneja,^{†,‡} Mudsser Azam,[§] Shadab Alam,[†] Ahmad Perwez,^{||} Ronan Maguire,[⊥] Umesh Yadava,[#] Kevin Kavanagh,[⊥] Constantin G. Daniliuc,[¶] M. Moshahid A. Rizvi,^{||} Qazi Mohd. Rizwanul Haq,[§] and Mohammad Abid^{*,†,‡}

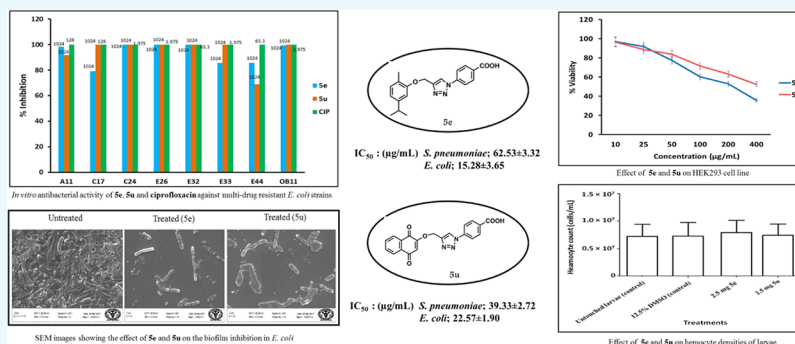
[†]Medicinal Chemistry Laboratory, Department of Biosciences, [‡]Department of Chemistry, [§]Microbiology Research Laboratory, Department of Biosciences, and ^{||}Genome Biology Laboratory, Department of Biosciences, Jamia Millia Islamia, Jamia Nagar, New Delhi 110025, India

[⊥]Department of Biology, Maynooth University, Co. Kildare ABC127, Ireland

[#]Department of Physics, Deen Dayal Upadhyay Gorakhpur University, Gorakhpur, Uttar Pradesh 273009, India

[¶]Organisch-Chemisches Institut, Westfälische Wilhelm-Universität, Münster 48149, Germany

Supporting Information



ABSTRACT: Despite the vast availability of antibiotics, bacterial infections remain a leading cause of death worldwide. In an effort to enhance the armamentarium against resistant bacterial strains, 1,2,3-triazole (**5a–x**) and sulfonate (**7a–j**) analogues of natural bioactive precursors were designed and synthesized. Preliminary screening against two Gram-positive (*Streptococcus pneumoniae* and *Enterococcus faecalis*) and four Gram-negative bacterial strains (*Pseudomonas aeruginosa*, *Salmonella enterica*, *Klebsiella pneumoniae*, and *Escherichia coli*) was performed to assess the potency of these analogues as antibacterial agents. Among all triazole analogues, **5e** (derived from carvacrol) and **5u** (derived from 2-hydroxy 1,4-naphthoquinone) bearing carboxylic acid functionality emerged as potent antibacterial agents against *S. pneumoniae* (IC_{50} : 62.53 and 39.33 μ g/mL), *E. faecalis* (IC_{50} : 36.66 and 61.09 μ g/mL), and *E. coli* (IC_{50} : 15.28 and 22.57 μ g/mL). Furthermore, **5e** and **5u** also demonstrated moderate efficacy against multidrug-resistant *E. coli* strains and were therefore selected for further biological studies. Compound **5e** in combination with ciprofloxacin displayed a synergistic effect on multidrug-resistant *E. coli* MRA11 and MRC17 strains, whereas compound **5u** was selective against *E. coli* MRA11 strain. Growth kinetic studies on *S. pneumoniae* and *E. coli* treated with **5e** and **5u** showed an extended lag phase. **5e** and **5u** did not show significant cytotoxicity up to 100 μ g/mL concentration on human embryonic kidney (HEK293) cells. Transmission electron microscopic (TEM) analysis of bacterial cells (*S. pneumoniae* and *E. coli*) exposed to **5e** and **5u** clearly showed morphological changes and damaged cell walls. Moreover, these compounds also significantly inhibited biofilm formation in *S. pneumoniae* and *E. coli* strains, which was visualized by scanning electron microscopic (SEM) analysis. Treatment of larvae of *Galleria mellonella* (an in vivo model for antimicrobial studies) with **5e** and **5u** did not cause an alteration in the hemocyte density, thereby indicating lack of an immune response, and were nontoxic up to a concentration of 2.5 mg/mL.

1. INTRODUCTION

The rising levels of multidrug-resistant (MDR) bacteria coupled with the scarcity of upcoming antibiotics have emerged as one of the most critical threats to public health in the 21st century.¹ Moreover, inappropriate use of available antibiotics has further worsened the situation, making previously treatable infections untreatable. As a result, efficacy

of the available antibiotics is diminishing at a faster rate.² MDR bacteria are responsible for infecting at least 2 million people annually along with the fatalities of at least 90 000 people in

Received: March 27, 2018

Accepted: June 8, 2018

Published: June 26, 2018

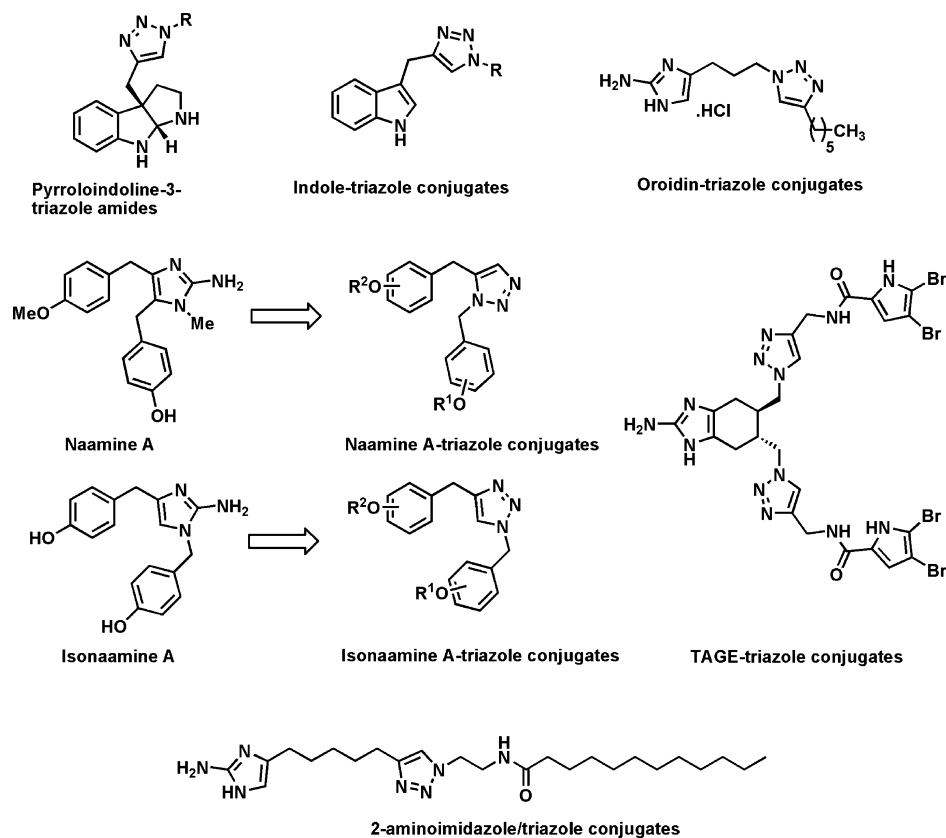


Figure 1. Natural product-based 1,2,3-triazole analogues as anti-biofilm agents.

the United States alone.³ Therefore, it has been recognized as one of the top three threats by the World Health Organization (WHO).⁴ A recent report by the Center for Disease Control and Prevention (CDC) suggested that we are at the verge of entering the “post-antibiotic era”.⁵ Thus, the development of antimicrobials with novel modes of action to inhibit bacterial infections is desperately required.

One of the most prominent features adopted by bacteria to develop resistance toward antibiotics is the formation of biofilms.⁶ Biofilms are highly hydrated organized structures, usually attached to both biotic and abiotic surfaces, multicellular communities of cells encased within the self-produced protective extracellular matrix. The biofilm-producing bacteria exhibit multifold resistance to conventional antibiotics and less susceptibility to host immune defenses and the external stresses.⁷ Biofilm-associated diseases such as cystic fibrosis pneumonia, periodontitis, prostatitis, recurrent urinary tract infection, and food-borne illnesses are posing serious threats to human health.⁸ Moreover, clogged filtration membranes, corroded pipes, or fouled immersed marine surfaces, which act as a source for pathogens in water and food processing, are other issues associated with biofilms.⁹

While a number of strategies are underway to develop antimicrobials with the ability to inhibit biofilm formation, modification of natural products has been proved to be a promising approach. Various literature reports have cited the role of natural products and their derivatives in the inhibition of biofilm formation. The incorporation of a triazole moiety to the naturally occurring compounds has resulted in potent antimicrobial analogues. For example, flustramine C-inspired pyrroloindoline-3-triazole amides,¹⁰ indole-triazole amide conjugates,¹¹ oroidin-triazole conjugates,¹² 2-aminoimidazole-

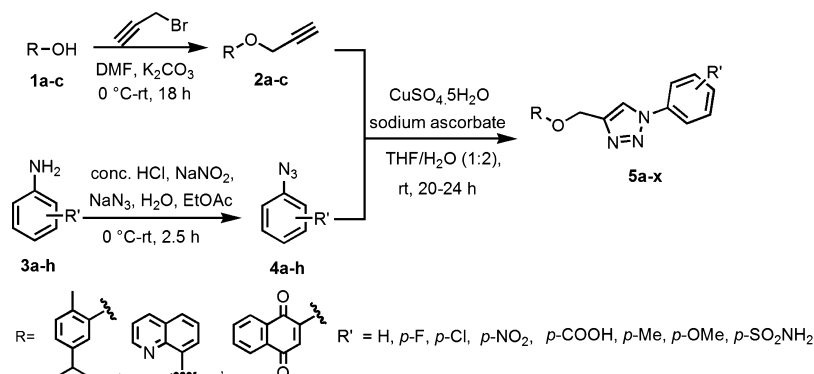
triazole conjugates,¹³ TAGE-triazole conjugates,¹⁴ pyrazolo-[3,4-*b*]pyridine-triazole conjugates,¹⁵ triazole containing naamine A and isonaamine A mimics,¹⁶ and triazole derivatives of geraniol and farnesol¹⁷ were found to inhibit the biofilm formation of several Gram-negative and Gram-positive bacteria (Figure 1).

Inspired by the significance of incorporation of 1,2,3-triazole functionality in the natural scaffold and in continuation of search for potent antimicrobial agents,^{18–21} we used hydroxyl-containing natural bioactive precursors including carvacrol, naphthoquinone, and 8-hydroxyquinoline for the modification. We also incorporated sulfonate onto these natural alcohols for comparison and screened all analogues against all tested bacterial strains. Compared to their natural precursors, compounds **5e** and **5u** showed significantly improved IC₅₀ values against *S. pneumoniae*, *E. faecalis*, and *E. coli*. Growth kinetic studies performed on *S. pneumoniae* and *E. coli* treated with lead inhibitors (**5e** and **5u**) showed their bacteriostatic nature. Importantly, these compounds strongly inhibit the formation of biofilm in the *S. pneumoniae* and *E. coli* strains and showed moderate potency against the resistant *E. coli* isolates. Furthermore, the selected compounds (**5e** and **5u**) were also subjected to in vitro (hemolysis and cytotoxicity assays) as well as in vivo toxicity assays on *G. mellonella* and found to be nontoxic. The study revealed that **5e** and **5u** provide a suitable core to be exploited for further structure–activity relationship (SAR) studies to develop potent antibacterial agents.

2. RESULTS AND DISCUSSION

2.1. Chemistry. The 1,2,3-triazole analogues (**5a–x**) of natural precursors were synthesized using the general synthesis approach, as shown in Scheme 1. Commercially available

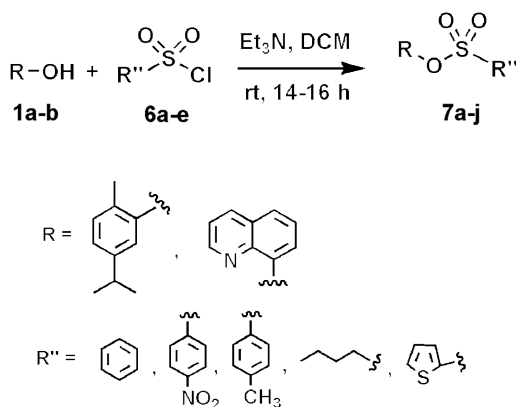
Scheme 1. Synthesis of 1,2,3-Triazole Derivatives of Natural Precursors



carvacrol (**1a**), 8-hydroxyquinoline (**1b**), and 2-hydroxy-1,4-naphthoquinone (**1c**) were propargylated in the presence of propargyl bromide and potassium carbonate to yield corresponding alkyne (**2a–c**). In another set of reaction, variously substituted aniline bearing electron-withdrawing/electron-donating groups (**3a–h**) were converted into their corresponding azides (**4a–h**) via diazotization using sodium nitrite and hydrochloric acid followed by sodium azide treatment. Finally, azide (**4a–h**) and alkyne (**2a–c**) underwent Cu(I)-catalyzed [3 + 2] cycloaddition reaction in the presence of catalytic amount of $\text{CuSO}_4 \cdot 5\text{H}_2\text{O}$ and sodium ascorbate in tetrahydrofuran (THF)/ H_2O (1:2) mixture to yield the title compounds (**5a–x**) in quantitative yields (Scheme 1).

For the synthesis of sulfonic esters, natural precursors (**1a–b**) were treated with aryl/heteroaryl/aliphatic sulfonyl chlorides (**6a–e**) in the presence of triethylamine base to yield sulfonate derivatives (**7a–j**) in quantitative yield (Scheme 2). All intermediates and title compounds (**5a–x**)

Scheme 2. Synthesis of Sulfonic Esters of Natural Precursors



and (**7a–j**) were well characterized using multi spectroscopic techniques, and purity was established by liquid chromatography (LC)–mass spectrometry (MS). Single crystal structures of 1,2,3-triazole derivatives (**5c** and **5f**) and sulfonic ester derivatives (**7g** and **7h**) were also recorded to further confirm the proposed structures.

2.2. X-ray Crystallographic Analysis. Single X-ray crystal structure analysis of 1,2,3-triazole derivatives (**5c** and **5f**) and sulfonic ester derivatives (**7g** and **7h**) was done to support structural analysis data. The crystal data and structure refinement details are presented in Table 1. A colorless crystal

of compound **5c** ($\text{C}_{19}\text{H}_{20}\text{ClN}_3\text{O}$), with approximate dimensions of $0.18 \times 0.10 \times 0.03 \text{ mm}^3$, was used for X-ray crystallographic analysis. The compound crystallized in a triclinic crystal system with the space group $P\bar{1}$ (Figure 2A). The unit cell contains two molecules with similar conformations, through which strong C–H \cdots N hydrogen bonds (C1A–H1A \cdots N2B 2.611 Å; C1B–H1B \cdots N2A 2.430 Å; C22A–H22A \cdots N3B 2.361 Å; C22B–H22B \cdots N3A 2.488 Å) generate linear chains along the *a*-axis with alternative orientation of A and B molecules (Figure 2B). Moreover, the crystal packing of **5c** presents the formation of additional C–H \cdots π interaction between the molecules (C3A–H3A \cdots C24A 2.734 Å) and C–H \cdots O interactions between the molecules (C12B–H12E \cdots O1B 2.688 Å). These interactions led to the formation of dimeric units (see Figure S1 in the Supporting Information).

Figure 2C represents the XP diagram of the compound **5f** with 50% probability level of thermal ellipsoids. The structure of compound **5f** ($\text{C}_{20}\text{H}_{23}\text{N}_3\text{O}$), a colorless platelike specimen, with approximate dimensions of $0.072 \times 0.233 \times 0.255 \text{ mm}^3$, was elucidated by X-ray crystallographic analysis. The crystal structure analysis revealed that it crystallizes in a monoclinic crystal system with the space group $P2_1/c$. In the packing diagram of **5f**, linear chains along the *b*-axis containing a double layer of alternating molecules were observed (Figure 2D). These chains are formed via C–H \cdots N hydrogen bonds and C–H \cdots π and $\pi\cdots\pi$ interactions. The shortest distance between the triazole derivative units is 3.392 Å and represents the centroid distance Cg1 \cdots Cg1. Two types of C–H \cdots N hydrogen bonds were found, one between two neighbored triazole units and the second type between one triazole ring and the phenyl substituent at N1 atom (C1–H1 \cdots N2 2.381 Å; C22–H22 \cdots N3 2.641 Å). In addition, C–H \cdots π interaction involving two phenoxy substituents (C13–H13 \cdots Cg2 2.683 Å) is contributing to the stability of this packing diagram. The resulted double layer chains are along the *c*-axis connected via $\pi\cdots\pi$ interactions between the triazole ring and the phenyl substituent (Cg3 \cdots Cg4 3.408 Å) (see Figure S2 in the Supporting Information).

X-ray crystallographic analysis of compound **7g** ($\text{C}_{15}\text{H}_{10}\text{N}_2\text{O}_5\text{S}$), a colorless needlelike specimen, of approximate dimensions $0.092 \times 0.169 \times 0.322 \text{ mm}^3$ revealed that it crystallizes in a monoclinic crystal system with the space group $P2_1/c$. The XP diagram of compound **7g** with ellipsoids drawn at a 50% probability level along with the atomic numbering scheme is shown in Figure 3A. In the packing diagram, a complex three-dimensional (3D) network involving intermolecular C–H \cdots O and $\pi\cdots\pi$ interactions was found. The partial

Table 1. Crystal Data and Structure Refinement Details for 5c, 5f, 7g, and 7h

identification code	5c	5f	7g	7h
formula	C ₁₉ H ₂₀ ClN ₃ O	C ₂₀ H ₂₃ N ₃ O	C ₁₅ H ₁₀ N ₂ O ₃ S	C ₁₆ H ₁₃ NO ₃ S
M _w (g/mol)	341.83	321.41	330.31	299.33
d _{calcd} (g cm ⁻³)	1.268	1.219	1.589	1.455
crystal size (mm)	0.18 × 0.10 × 0.03	0.072 × 0.233 × 0.255	0.092 × 0.169 × 0.322	0.020 × 0.100 × 0.160
T/K	223(2)	104(2)	104(2)	100(2)
λ (Å)	0.71073	0.71073	0.71073	1.54178
F(000)	720	688	680	312
crystal system	triclinic	monoclinic	monoclinic	triclinic
space group	P $\bar{1}$	P2 ₁ /c	P2 ₁ /c	P $\bar{1}$
a (Å)	11.0378(3)	20.1641(12)	10.3165(4)	8.9865(3)
b (Å)	11.8494(4)	5.4625(3)	11.1535(4)	9.2432(3)
c (Å)	13.7117(5)	16.6110(10)	12.6841(5)	9.3299(3)
α (deg)	92.880(2)	90	90	66.983(2)
β (deg)	90.142(2)	106.857(2)	108.871(2)	79.673(2)
γ (deg)	91.245(2)	90	90	73.972(2)
V (Å ³)	1790.67(10)	1751.02(18)	1381.05(9)	683.32(4)
Z	4	4	4	2
θ range (deg)	4.11–25.00	2.47–26.37	2.49–27.51	5.14–68.09
collected reflections	8979	33 271	21 467	9610
unique reflections; R _{int}	6136 [R _{int} = 0.0381]	3567 [R _{int} = 0.0611]	3169 [R _{int} = 0.0568]	2382 [R _{int} = 0.0348]
μ/mm ⁻¹	0.223	0.077	0.264	2.196
R(F _o), [I > 2σ(I)]	0.0787	0.0672	0.0354	0.0322
R _w (F _o ²) (all data)	0.1177	0.0821	0.0486	0.0360
GoF (F ²)	1.101	1.167	1.062	1.083
Δρ [e Å ⁻³]	0.298/−0.249	0.269/−0.295	0.337/−0.477	0.316/−0.363
CCDC number	1516149	1516150	1516148	1516147

overlapping mode between the nitrobenzene substituent and the quinoline unit (Cg1...Cg2 3.288 Å) combined with C–H...O hydrogen bonds involving the sulfonate unit leads to the formation of wave chains along the *b*-axis (Figure 3B). Additional C–H...O hydrogen bonds of the nitro and sulfonate groups complete the 3D network (see Table S17 in the Supporting Information).

X-ray crystallographic analysis was used to unambiguously confirm the structure of compound 7h (C₁₆H₁₃NO₃S), a colorless platelike specimen, with approximate dimensions of 0.020 × 0.100 × 0.160 mm³. Crystal structure analysis of compound 7h revealed that it crystallizes in a triclinic crystal system with the space group P $\bar{1}$. The XP diagram of compound 7h with ellipsoids drawn at a 50% probability level along with atomic numbering scheme is shown in Figure 3C. For compound 7h, a 3D network involving C–H...O, C–H...N, C–H...π, and π...π interactions was observed. In contrast to the packing diagram of 7h, a lower overlapping mode between quinoline and *p*-tolyl groups was observed. The strongest interactions (C–H...O hydrogen bonds) were found between sulfonate and quinoline groups (C8–H8...O1 2.466 Å) and are leading to the formation of dimeric units. These dimers are connected along *ab*-diagonal through weak π...π interactions to linear chains (Figure 3D). Additional interactions (C–H...O, C–H...π, and C–H...N) are stabilizing the structure of this compound (see Table S21 in the Supporting Information).

2.3. In Vitro Antibacterial Activity. All natural precursors and their triazole/sulfonate analogues were primarily screened for antibacterial activity against Gram-positive (*S. pneumoniae* and *E. faecalis*) and Gram-negative (*P. aeruginosa*, *S. enterica*, *K. pneumoniae*, and *E. coli*) sensitive bacterial strains. Ciprofloxacin (CIP) was used as a reference drug, and the results are presented in terms of IC₅₀ values in Table 2. The results

showed that compounds exhibited moderate to potent antibacterial activity against both Gram-positive and Gram-negative bacteria. Moreover, as compared to natural precursors, compounds 5e and 5u with *p*-carboxylic acid substitution emerged as potent inhibitors of *E. coli* with IC₅₀ values of 15.28 and 22.57 μg/mL, respectively. Moreover, these compounds also inhibited the growth of *S. pneumoniae* (62.53 and 39.33 μg/mL, respectively) as well as *E. faecalis* with IC₅₀ values of 36.66 and 61.09 μg/mL, respectively. It was observed that the corresponding analogue of quinoline, 5m, exhibited moderate inhibitory effect on the same bacterial strains (*S. pneumoniae*, *E. faecalis*, and *E. coli*). The analogues of carvacrol (5a) and quinoline (5i) with unsubstituted phenyl substituent clearly lost their potential against all bacterial strains, whereas the corresponding analogue of naphthoquinone (5q) displayed IC₅₀ values of 96.99, 101.23, and 99.53 μg/mL against *S. pneumoniae*, *E. faecalis*, and *E. coli*, respectively. None of the halogen-substituted (*p*-fluoro and *p*-chloro substitution) compounds exhibited potency against any of the bacterial strains except compound 5r with *p*-fluoro substitution, which showed a modest effect on *S. pneumoniae* and *E. coli* with IC₅₀ values of 133.86 and 164.78 μg/mL, respectively. Except the moderate effect of compound 5d on *K. pneumoniae* (IC₅₀ = 121.83 μg/mL), none of the *p*-nitro-substituted analogues exhibited potency against any of the strains tested. The analogues bearing electron-donating substituents such as *p*-methyl and *p*-methoxy exhibited better inhibition of all bacterial strains in comparison to halogen-substituted (*p*-fluoro and *p*-chloro substitution) analogues, where the activity was considerably lost against all strains. Among all *p*-sulfonamide-substituted analogues, 5x moderately inhibited the growth of *S. pneumoniae* and *E. coli* strains with IC₅₀ values of 85.23 and 103.54 μg/mL, respectively, whereas

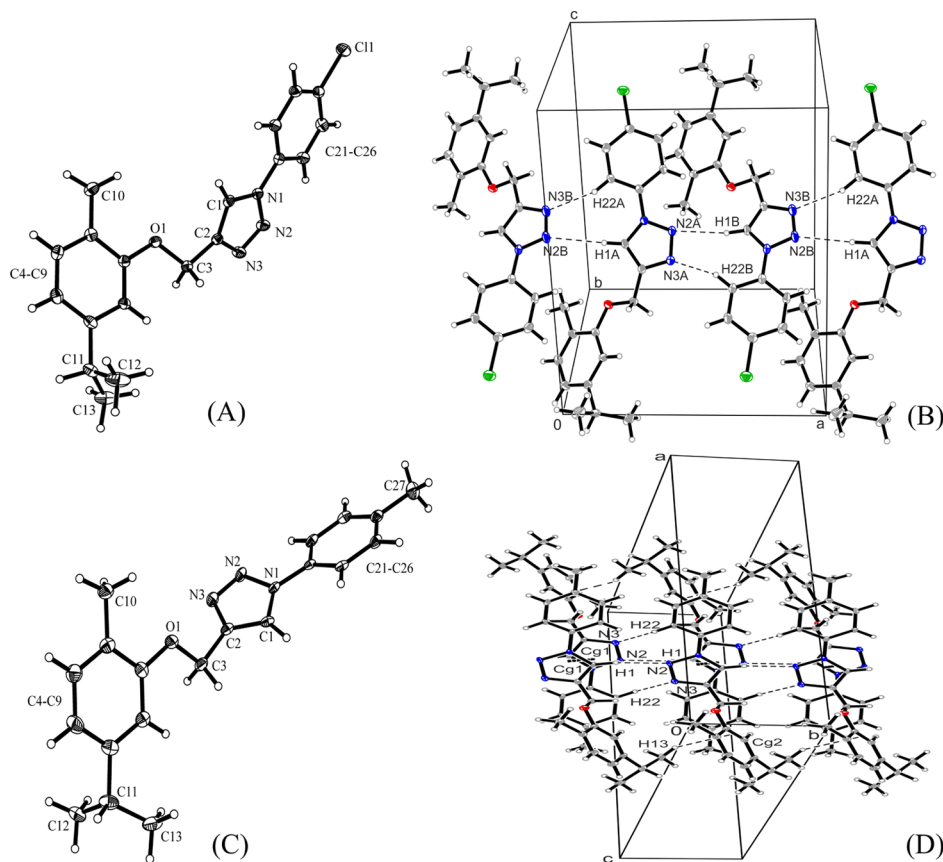


Figure 2. (A) XP diagram of compound **5c** with atomic labeling scheme (50% probability level of thermal ellipsoids); (B) excerpt of the packing diagram of **5c** representing the chain formation along the *a*-axis via CH...N interactions; (C) XP diagram of compound **5f** with atomic labeling scheme (50% probability level of thermal ellipsoids); and (D) linear double-layer chain formation through CH...N interactions along the *b*-axis in **5f**.

it exhibited potent effect on *E. faecalis* with an IC_{50} value of $39.23 \mu\text{g/mL}$. Among all sulfonic ester analogues (**7a–j**), the compound derived from carvacrol (**7a**) with an unsubstituted phenyl ring displayed a moderate activity against *E. coli* and *K. pneumoniae* with IC_{50} values of 112.94 and $117.09 \mu\text{g/mL}$, respectively. Compound **7d** with *n*-butyl tail exhibited an IC_{50} value of $95.54 \mu\text{g/mL}$ against *K. pneumoniae*. Compounds **7d** and **7e** with a thiophenyl ring displayed moderate potency against *P. aeruginosa* with IC_{50} values of 118.45 and $119.04 \mu\text{g/mL}$, respectively. None of the sulfonic esters derived from quinoline exhibited a significant effect on any of the bacterial strains. The *in vitro* antibacterial evaluation results showed the importance of incorporation of a triazole scaffold over sulfonic esters.

On the basis of the results obtained on sensitive bacterial strains, compounds **5e** and **5u** were selected for further screening on eight multidrug-resistant *E. coli* strains. It was observed that at $1024 \mu\text{g/mL}$ concentration [minimum inhibitory concentration (MIC)], compounds **5e** exhibited more than 95% inhibition of *E. coli* MRA11, MRC24, MRAE26, MRAE32, and MROB11 strains, whereas at the same concentration, it caused 79, 86, and 86% inhibition of *E. coli* MRC17, MRAE33, and MRAE44 strains, respectively. Compound **5u** at the MIC value ($1024 \mu\text{g/mL}$) caused nearly 100% inhibition of the growth of MRC17, MRC24, MRAE26, MRAE32, MRAE33, and MROB11 strains, whereas it caused only 70% inhibition of MRAE44 growth, showing moderate efficacy on this strain. **5u** was also effective on MRA11 strain,

causing more than 90% inhibition of growth, indicating moderate efficacy of these compounds in comparison to CIP, which showed almost 100% inhibition at a concentration lower than those of the compounds (Figure 4). These compounds were further evaluated for their *in vitro* synergistic effects in combination with CIP against *E. coli* MRA11, MRC17, and MRAE33 strains. The results indicated that antibacterial activity of **5e** against all three strains was significantly enhanced when used in combination with CIP. Compound **5u** in combination with CIP exhibited a significant improvement in antibacterial activity against *E. coli* MRAE33, whereas it exhibited a moderate activity against *E. coli* MRA11. The fractional inhibitory concentration index (FICI) values of compound **5e** were 0.03 against *E. coli* MRA11 and MRC17 strains, indicating high synergistic effect, whereas compound **5u** exhibited partial synergy against *E. coli* MRA11 with an FICI value of 0.62. None of the compound exhibited synergistic effect in combination with CIP against *E. coli* MRAE33 (Tables 3 and 4). These results prompted us to explore the effect of these inhibitors (**5e** and **5u**) on the growth kinetics of *S. pneumoniae* and *E. coli*. The kinetic studies showed that both compounds exhibited inhibitory effects on the growth pattern of *S. pneumoniae* and *E. coli* strains. Compound **5e** was found to be more potent as it effectively inhibited the growth of *S. pneumoniae* even at a sub-MIC concentration ($62.5 \mu\text{g/mL}$). Furthermore, no significant growth of *E. coli* was observed at MIC and 2MIC concentrations up to 22 h of incubation, whereas at a sub-

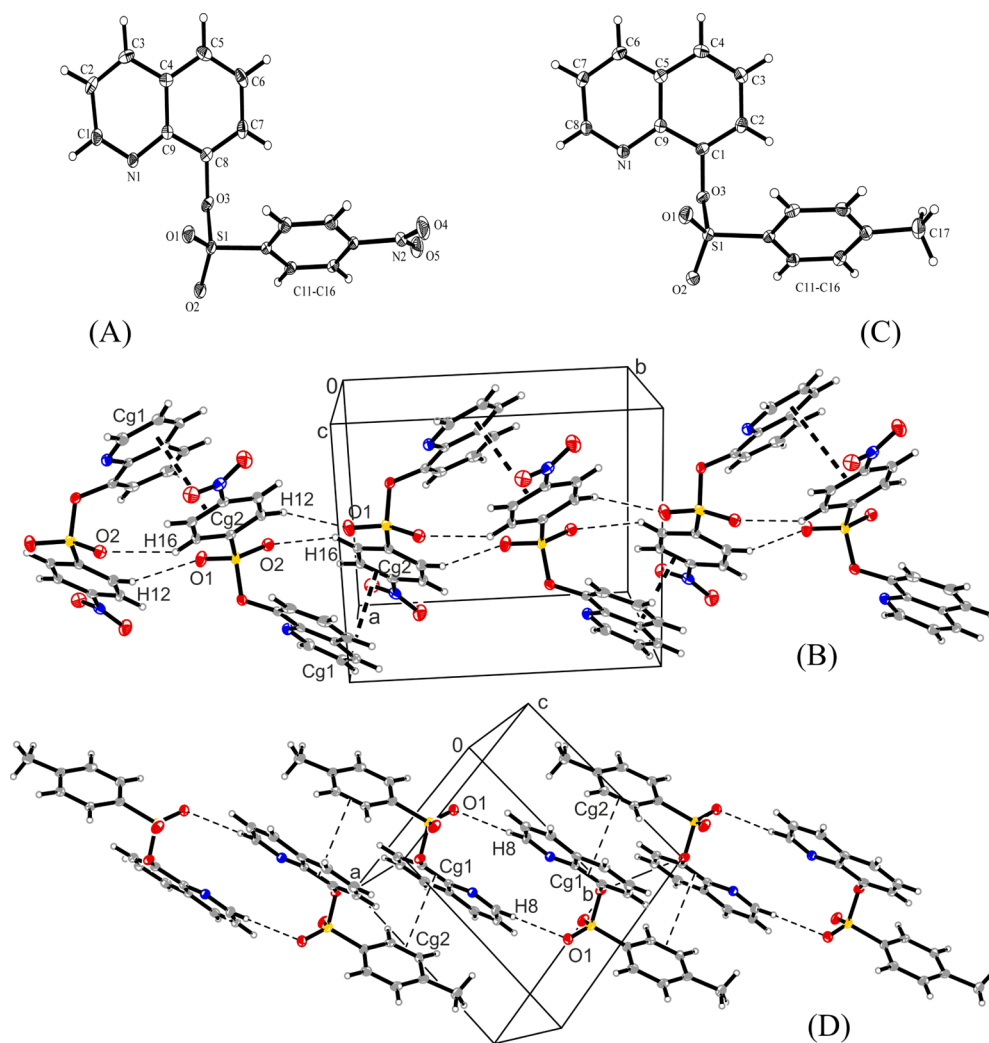


Figure 3. (A) XP diagram of compound **7g** with atomic labeling scheme (50% probability level of thermal ellipsoids); (B) wave chain along the *b*-axis formed via $\pi\cdots\pi$ and $\text{CH}\cdots\text{O}$ interactions in the packing diagram of **7g**; (C) XP diagram of compound **7h** with atomic labeling scheme (50% probability level of thermal ellipsoids); and (D) linear chain of dimeric units along *ab*-diagonal formed via $\text{CH}\cdots\text{O}$ and $\pi\cdots\pi$ interactions in the packing diagram of **7h**.

MIC concentration, a suppressed growth was observed with a lag phase of approximately 6 h. Compound **5u** was found to be less effective as growth in *S. pneumoniae* could be observed in 8 and 9 h at sub-MIC and MIC concentrations, respectively, whereas in the case of *E. coli*, growth was observed at 6 and 9 h at sub-MIC and MIC concentrations of **5u**. An increase in turbidity representing bacterial growth post 22 h in all test cultures indicated the bacteriostatic nature of **5e** and **5u** (Figure 5).

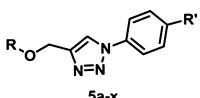
2.4. TEM Analysis of *S. pneumoniae* and *E. coli* Cells Treated with **5e and **5u**.** TEM analysis was performed to check the effect of **5e** and **5u** on the morphology of *S. pneumoniae* and *E. coli* cells. The cell culture of *E. coli* treated with MIC concn of **5e** and **5u** and untreated cells (control) were used for TEM analysis. It was observed that the treated cells showed moderate to severe cellular deformities, whereas untreated cells were normal in shape with an intact cell wall. The treatment of bacterial cells with **5e** and **5u** significantly damaged the cell wall, resulting in the loss of integrity and cytosolic oozing. The degraded cell wall of bacteria observed in the TEM micrographs proposes the bactericidal activity of test

compounds. Their antibacterial mode of action needs to be further characterized (Figure 6).

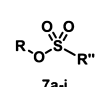
2.5. Effect of **5e and **5u** on the Biofilm Formation.**
2.5.1. Assessment of Anti-Biofilm Activity by Tetrazolium Salt (XTT) Reduction Assay. The effect of lead compounds (**5e** and **5u**) on biofilm formation was determined using *E. coli* and *S. pneumoniae* strains. The compounds exhibited significant inhibition of biofilm formation in both the strains. Compounds **5e** and **5u** inhibited the biofilm formation in *E. coli* by 95.23 and 92.26% at a concentration of 125 $\mu\text{g}/\text{mL}$ (2MIC) of **5e** and 250 $\mu\text{g}/\text{mL}$ (2MIC) of **5u**, respectively. Similarly, in the case of *S. pneumoniae*, 92.26 and 100% inhibition was observed at a concentration of 250 $\mu\text{g}/\text{mL}$ (2MIC) of **5e** and **5u**, respectively. From the results, it was concluded that both compounds could be further customized to develop as potent anti-biofilm agents (Figure 7).

2.5.2. Assessment of Anti-Biofilm Activity by Crystal Violet Assay. Anti-biofilm activity of the lead compounds (**5e** and **5u**) on *E. coli* and *S. pneumoniae* strains was further determined by crystal-violet assay. Compound **5e** inhibited the biofilm formation in *E. coli* by 94.32% at 125 $\mu\text{g}/\text{mL}$ (2MIC) concentration and in *S. pneumoniae* by 93.36% at a

Table 2. In Vitro Antibacterial Activity (IC_{50}) of 1,2,3-Triazole and Sulfonic Esters of Natural Precursors ($\mu\text{g/mL}$)^a



5a-x



7a-j

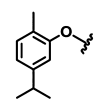
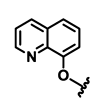
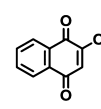
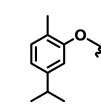
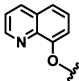
Comp.	R	R'/R''	<i>S. pneumoniae</i>	<i>E. fecalis</i>	<i>E. coli</i>	<i>K. pneumoniae</i>	<i>P. aeruginosa</i>	<i>S. enterica</i>
1a	Carvacrol		95.2±3.30	68.16±2.20	96.18±3.72	61.91±0.82	43.93±2.77	95.65±1.15
5a		H	472.83±3.47	653.72±4.49	249.41±2.45	161.56±4.32	655.46±6.85	425.5±3.41
5b		F	314.98±3.56	333.94±4.29	1580.64±6.09	211.23±3.94	244.55±4.67	544.49±3.14
5c		Cl	305.97±3.56	235.44±3.96	654.84±2.95	205.89±5.92	254.33±5.35	451.42±6.88
5d		NO ₂	494.38±3.87	239.69±5.63	532.28±4.85	121.83±1.18	148.72±4.97	473.28±2.24
5e		COOH	62.53±3.32	36.66±1.48	15.28±3.65	261.22±4.10	134.68±5.32	402.22±1.97
5f		Me	375.33±4.39	243.62±2.28	288.76±3.81	246.09±3.86	231.29±5.25	304.86±3.00
5g		OMe	305.04±3.43	184.04±2.92	320.28±6.93	483.01±5.10	168.85±3.46	343.74±2.09
5h		SO ₂ NH ₂	572.81±5.74	161.78±3.89	288.94±3.81	601.56±6.87	406.18±4.05	1291.10±3.45
1b	8-Hydroxyquinoline		15.65±2.34	42.50±1.56	49.50±2.34	49.50±2.34	87.56±1.23	17.23±1.28
5i		H	261.75±4.96	202.24±3.19	407.63±3.17	400.92±4.73	724.68±3.22	555.45±4.00
5j		F	377.21±4.57	613.82±3.60	404.92±4.30	1228.39±7.12	844.06±4.95	640.64±6.60
5k		Cl	273.86±4.91	474.40±2.95	469.96±6.71	554.24±6.78	1437.57±5.58	355.87±3.80
5l		NO ₂	174.95±3.98	1291.73±6.75	664.30±5.79	554.28±6.05	311.66±4.02	309.18±3.08
5m		COOH	105.96±3.76	134.00±4.22	108.50±3.08	215.38±5.51	575.66±3.76	235.98±4.79
5n		Me	112.65±2.37	143.25±2.99	175.64±4.08	268.48±2.95	133.43±4.42	135.85±3.69
5o		OMe	164.45±4.45	356.17±4.77	375.66±3.47	336.21±4.77	256.42±5.52	186.99±2.68
5p		SO ₂ NH ₂	721.22±7.74	1707.62±6.07	880.31±5.56	866.46±3.85	314.02±3.86	468.89±4.61
1c	2-hydroxynaphthoquinone		87.16±3.41	96.01±2.26	179.1±1.42	123.40±2.55	73.8±0.89	86.23±2.09
5q		H	96.99±1.01	101.23±4.28	99.53±2.43	223.45±5.65	324.71±4.53	224.56±5.31
5r		F	133.86±5.63	1063.56±6.98	164.78±3.89	672.45±4.93	417.51±6.54	493.86±3.48
5s		Cl	1186.51±6.65	694.75±3.54	305.79±3.66	347.74±5.64	387.79±7.50	780.23±5.67
5t		NO ₂	348.66±3.39	502.24±4.48	395.65±5.98	369.92±5.22	323.97±1.92	201.53±5.08
5u		COOH	39.33±2.72	61.09±4.39	22.57±1.90	267.1±5.74	348.08±3.95	251.19±5.76
5v		Me	106.15±2.23	112.88±3.47	223.57±5.85	220.43±4.79	263.48±5.37	160.36±4.81
5w		OMe	105.26±3.70	107.34±3.62	313.98±4.99	136.98±2.30	279.5±2.73	171.54±2.46
5x		SO ₂ NH ₂	85.23±2.14	39.23±3.24	103.54±4.78	256.28±4.01	223.54±5.23	246.72±5.67
7a		Ph	173.77±3.53	240.72±4.79	112.94±3.19	117.09±3.99	132.05±3.96	345.53±3.01
7b		4-NO ₂ Ph	886.71±5.94	245.24±3.31	176.00±4.42	463.44±5.72	138.73±5.77	237.38±5.45
7c		4-CH ₃ Ph	355.54±5.20	220.48±7.74	316.96±4.43	279.41±5.72	145.14±3.94	236.8±3.13
7d		n-butyl	228.76±3.49	174.59±4.36	156.27±3.33	95.54±3.25	118.45±4.19	174.05±3.38
7e		thiophenyl	169.28±5.90	157.08±3.35	149.08±2.83	163.19±4.10	119.04±4.13	435.41±5.93

Table 2. continued

Comp.	R	R ¹ /R ²	<i>S. pneumoniae</i>	<i>E. fecalis</i>	<i>E. coli</i>	<i>K. pneumoniae</i>	<i>P. aeruginosa</i>	<i>S. enterica</i>
7f		Ph	222.89±5.23	263.15±4.35	276.88±4.09	340.48±5.56	324.05±6.66	585.31±4.08
7g		4-NO ₂ Ph	257.41±5.32	431.37±4.79	214.84±4.24	227.91±3.62	211.56±4.93	353.92±2.68
7h		4-CH ₃ Ph	317.12±3.35	148.88±4.17	133.41±2.85	121.85±4.79	176.85±3.77	407.28±2.81
7i		n-butyl	158.11±2.75	195.24±4.18	194.34±2.49	171.26±4.99	176.45±3.39	155.74±3.90
7j		thiophenyl	308.76±7.39	509.15±4.82	164.86±3.32	442.73±2.77	317.59±4.16	714.10±6.08
CIP			0.313	0.063	0.125	0.250	0.250	0.012

^aThe value obtained in at least three separate assays done in triplicate.

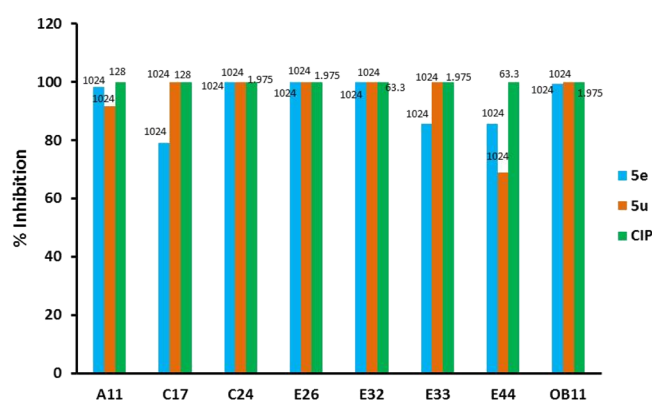


Figure 4. In vitro antibacterial activity of **5e**, **5u**, and CIP ($\mu\text{g/mL}$) against multidrug-resistant *E. coli* strains: MRA11, MRC17, MRC24, MRAE26, MRAE32, MRAE33, MRAE44, and MROB11. The numbers written above the respective columns correspond to the MIC concentrations of **5e**, **5u**, and CIP.

Table 3. In Vitro Synergistic Effect of **5e**

<i>E. coli</i> strain	MIC alone ($\mu\text{g/mL}$)		MIC in combination ($\mu\text{g/mL}$)		FICI ^a	mode of interaction
	5e	CIP	5e	CIP		
MRA11	1024	128	16	2	0.03	synergistic
MRC17	1024	128	16	2	0.03	synergistic
MRAE33	1024	2	16	2	1.02	indifferent

^aSynergy and antagonism were defined by $\text{FICI} \leq 0.5$ and >4 , respectively. Partially synergistic was denoted by $0.5 > \text{FICI} < 1$, and indifferent was defined by $1 < \text{FICI} \leq 4$.

Table 4. In Vitro Synergistic Antibacterial Activity of **5u**

<i>E. coli</i> strain	MIC alone ($\mu\text{g/mL}$)		MIC in combination ($\mu\text{g/mL}$)		FICI ^a	mode of interaction
	5u	CIP	5u	CIP		
MRA11	1024	128	512	16	0.62	partially synergistic
MRC17	1024	128	1024	64	1.50	indifferent
MRAE33	1024	2	16	2	1.02	indifferent

^aSynergy and antagonism were defined by $\text{FICI} \leq 0.5$ and >4 , respectively. Partially synergistic was denoted by $0.5 > \text{FICI} < 1$, and indifferent was defined by $1 < \text{FICI} \leq 4$.

concentration of $250 \mu\text{g/mL}$ (2MIC). Similarly, compound **5u** inhibited the biofilm formation by 77.26 and 98.28% in *E. coli* and in *S. pneumoniae*, respectively, at a concentration of 250

$\mu\text{g/mL}$ (2MIC) (Figure 7). To assess the viability of bacterial cells post treatment, colony forming unit (CFU) count was also performed (Table 5). The viability data showed that compounds **5e** and **5u** were able to reduce the colony formation of bacterial cells when compared with untreated counterparts. Analysis of biomass formation in control and treated samples demonstrated higher biomass formation in control samples. The OD₅₉₀ values presenting the biofilm formation via viable cells revealed maximum biomass in the control sample followed by samples treated with test compounds **5e** and **5u** followed by CIP-treated cells, thus showing a maximum antimicrobial activity (Figure 8).

2.5.3. Assessment of Biofilm Inhibition by SEM Analysis. SEM analysis was also carried out to validate the effect of lead compounds **5e** and **5u** on biofilm formation in *E. coli* strain. On exposure to the 2MIC concentration of **5e** and **5u**, significant inhibition of biofilm formation was observed in the treated cells. In untreated samples, the cells appeared in clusters with a polysaccharide matrix, which showed the formation of a biofilm, whereas cells treated with 2MIC concentration of **5e** showed scattered single cells with significant cell damage. Compound **5u**, although significantly effective in inhibiting biofilm formation, was less potent than **5e** as the cell integrity was lost to lesser extent in the latter case (Figure 9).

2.6. Toxicity Evaluation of Lead Compounds by in Vitro (MTT and Hemolytic Assay) and in Vivo (on *G. mellonella* Larvae) Studies. **2.6.1. Toxicity Studies by MTT and Hemolytic Assays.** The cytotoxicity of the lead inhibitors (**5e** and **5u**) was evaluated by MTT assay on HEK293 cells (Figure 10A). The results showed that both the compounds retained more than 75% cell viability at $50 \mu\text{g/mL}$ concentration but exhibited moderate toxicity at a concentration of $200 \mu\text{g/mL}$ (more than 50% cell viability). On increasing the concentration to $400 \mu\text{g/mL}$, cell viability further decreased, which indicated that the compounds possess some toxicity at higher concentrations. At the IC₅₀ concentration, these compounds could be considered nontoxic and thus can be further investigated for in vivo evaluation. To exclude any possible toxicity on human red blood cells (hRBCs), hemolytic assay was also performed with **5e** and **5u**. At $200 \mu\text{g/mL}$ concentration, compounds **5e** and **5u** caused only 9% cell lysis in comparison to 0.8% cell lysis caused by CIP at the same concentration. More interestingly, compounds **5e** and **5u** were found to exhibit insignificant toxicity up to $600 \mu\text{g/mL}$ with only 22 and 12% cell lysis, respectively (Figure 10B).

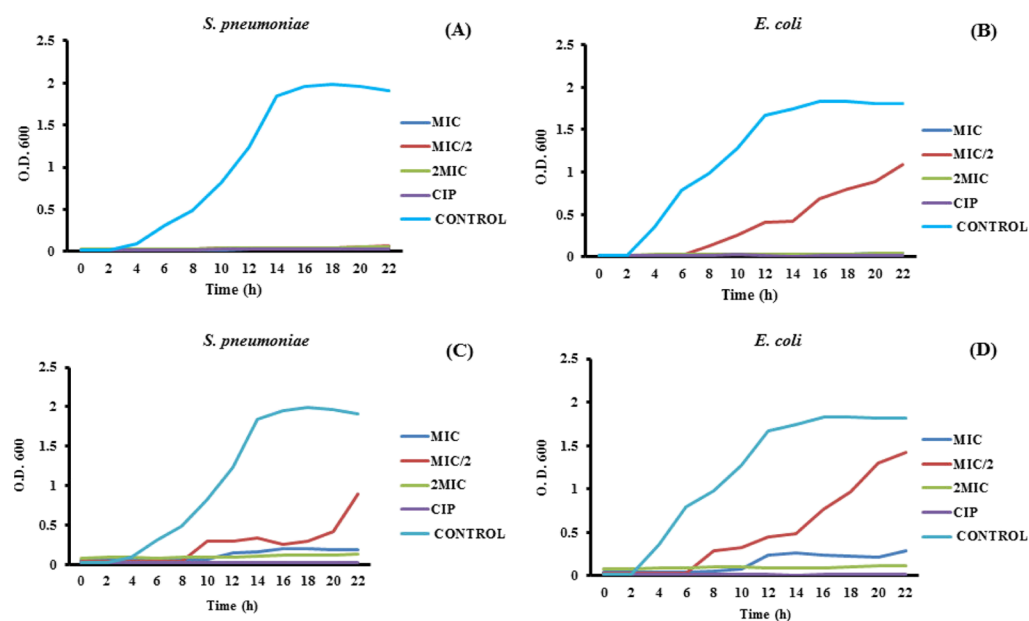


Figure 5. Growth kinetic studies under different concentrations of test compounds. (A,B) treated with **5e** and (C,D) treated with **5u**.

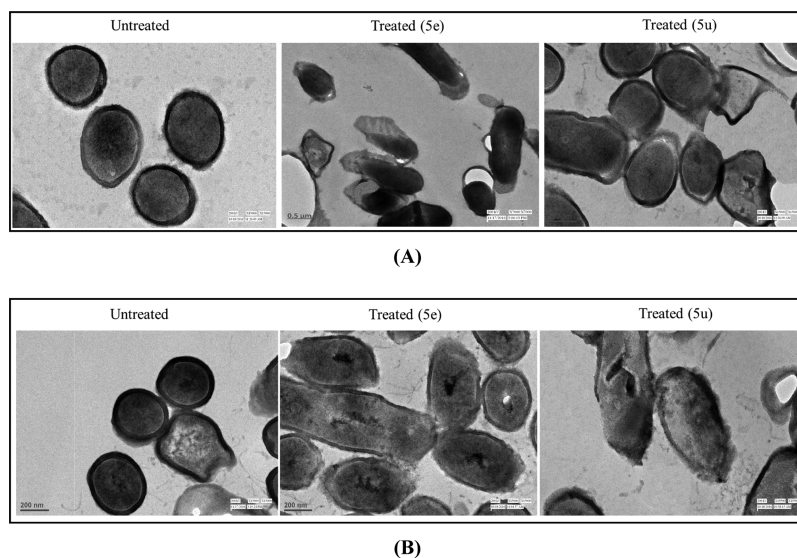


Figure 6. Representative transmission electron micrographs of (A) *E. coli* and (B) *S. pneumoniae* cells exposed to **5e** (62.5 and 125 $\mu\text{g}/\text{mL}$ concentrations, respectively) and **5u** (125 $\mu\text{g}/\text{mL}$ concentration) at their respective MICs.

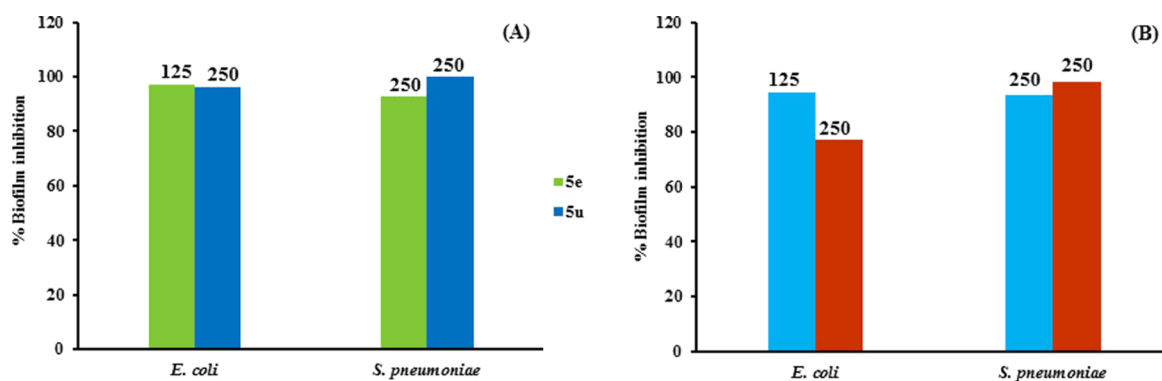
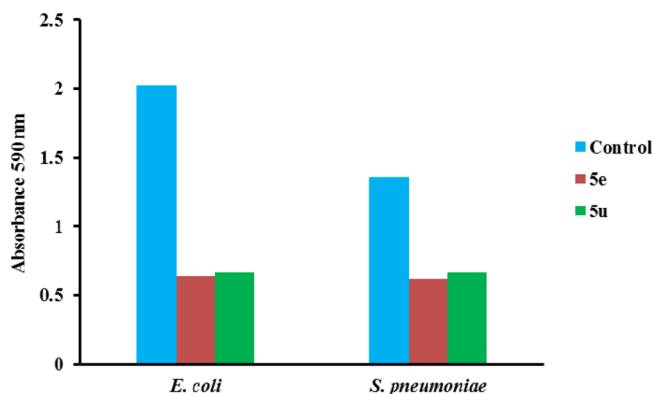


Figure 7. Percentage of biofilm inhibition in *E. coli* and *S. pneumoniae* on treatment with **5e** and **5u** using (A) XTT assay and (B) crystal violet assay. The numbers (125 and 250) written above the respective columns correspond to the 2MIC concentrations of **5e** and **5u**, respectively.

Table 5. CFUs of *E. coli* and *S. pneumoniae* Observed in Treated and Untreated Bacterial Cells

	<i>E. coli</i>	<i>S. pneumoniae</i>
control	1.67×10^5	1.1×10^4
CIP	2.0×10^4	5.0×10^3
5e	2.5×10^4	7.8×10^3
5u	2.7×10^4	6.0×10^3

**Figure 8.** Biomass determination in *E. coli* and *S. pneumoniae* at OD₅₉₀.

2.7. In Vivo Toxicity Evaluation of 5e and 5u on *G. mellonella* Larvae. Because immune response of insects exhibits remarkable similarities to the innate immune response of mammals, insects have been used as models for the evaluation of toxicity of antimicrobial drugs. It has been reported previously that *G. mellonella* has been utilized to assess the toxicity of novel antimicrobial drugs and the results showed a strong correlation with those obtained using mammals.²² An in vivo study on the larvae of *G. mellonella* showed that viability of the larvae was not affected up to the concentration of 2.5 mg/mL of test compounds (5e and 5u), indicating their nontoxic behavior towards the larvae (Figure 11A–C). Moreover, at the same concentration, hemocyte density of the larvae was not significantly affected, which indicated lack of an immune response (Figure 11D).

2.8. Absorption, Distribution, Metabolism, and Excretion (ADME) Profiling. The computational prediction of important physicochemical descriptors related to absorption, distribution, metabolism, and excretion properties represents a cost-effective strategy to filter out molecules at early stages of drug-discovery process.²³ Here, we did in silico physicochemical prediction for all analogues (5a–x and 7a–j) using QikProp version 3.2, Schrödinger software.²⁴ Particularly, we predicted total polar surface area, the number of rotatable bonds (NRB), aqueous solubility (QP log S), binding

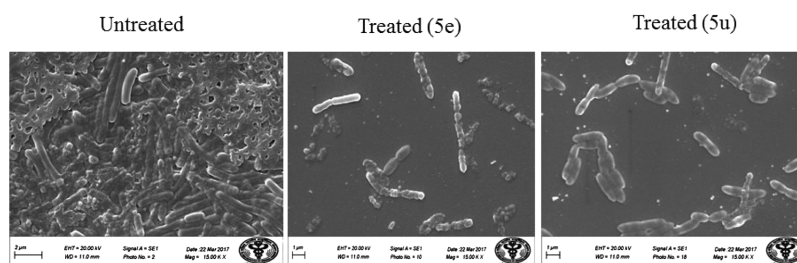
to human serum albumin (QP log K_{hsa}), brain/blood partition coefficient (QP log BB), Caco-2 and MDCK permeability, and estimation of % human oral absorption, which indicated the druglike characteristics of these compounds. In addition, Lipinski's parameters for drug-likeness were also calculated, which states that any orally active drugs should not violate more than one of its parameters.²⁵ These compounds follow Lipinski's rule of 5 and possessed moderate to good % human oral absorption. Therefore, these compounds have the potential to be carried forward for SAR and pharmacological investigations. All results of in silico physicochemical prediction are summarized in Table S1 (Supporting Information).

3. CONCLUSIONS

In summary, a novel series of 1,2,3-triazole/sulfonate analogues derived from natural bioactive alcohols were synthesized and evaluated for their potential as antibacterial agents against a panel of Gram-positive and Gram-negative bacterial strains. Most of the compounds displayed good to moderate antibacterial activity across the panel. Compounds 5e and 5u emerged as potent antibacterial agents against sensitive *S. pneumoniae*, *E. faecalis*, and *E. coli* strains as well as moderately effective against MDR *E. coli* strains. Compound 5e in combination with CIP showed a synergistic effect on MDR *E. coli* MRA11 and MRC17 strains, whereas compound 5u was selective against *E. coli* MRA11. Further, growth kinetic studies confirmed the bacteriostatic nature of the test compounds. TEM analysis showed that 5e and 5u caused significant cell wall damage and membrane disruption of bacterial cells (*S. pneumoniae* and *E. coli*), leading to cell death. Moreover, these compounds were also found to be potent anti-biofilm agents on *S. pneumoniae* and *E. coli* strains and exhibited non-cytotoxicity on the HEK293 cell line up to a concentration of 100 $\mu\text{g/mL}$. Besides, these compounds did not cause an alteration in the hemocyte density, indicating the lack of an immune response, and were nontoxic on the larvae of *G. mellonella* up to the concn of 2.5 mg/mL. Our study firmly supports further structural optimization of these compounds (5e and 5u) for the development of potent and safer antibacterial agents.

4. EXPERIMENTAL SECTION

4.1. Chemistry. All chemicals and solvents (analytical grade) were purchased from Sigma-Aldrich, USA. Thin-layer chromatographic analysis was carried out on precoated Merck silica gel 60 F₂₅₄ TLC aluminum sheets, and spots were visualized under UV light at 254 nm and I₂ vapor staining. IR spectra were recorded on an Agilent Cary 630 Fourier transform infrared spectrometer, and only major peaks are

**Figure 9.** SEM images showing biofilm inhibition in *E. coli*.

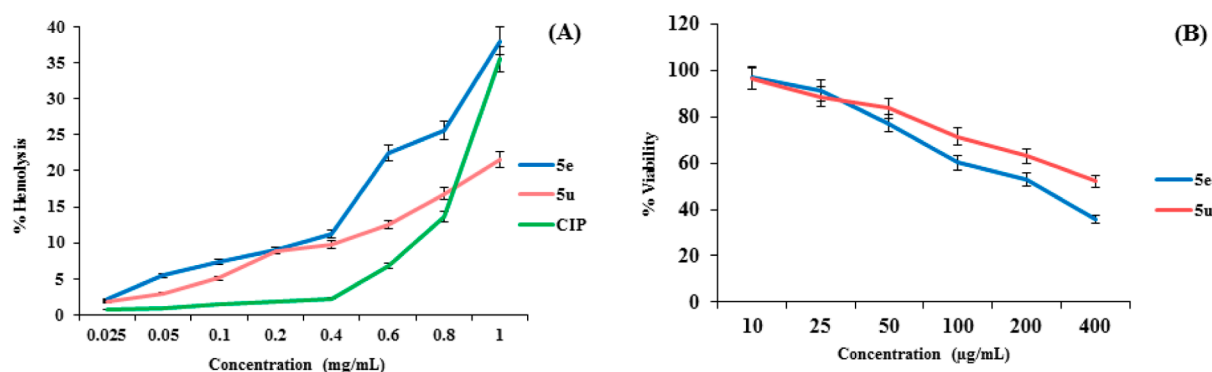


Figure 10. (A) Cell viability assay on HEK293 cell line and (B) hemolytic assay for compounds **5e**, **5u**, and CIP on hRBCs.

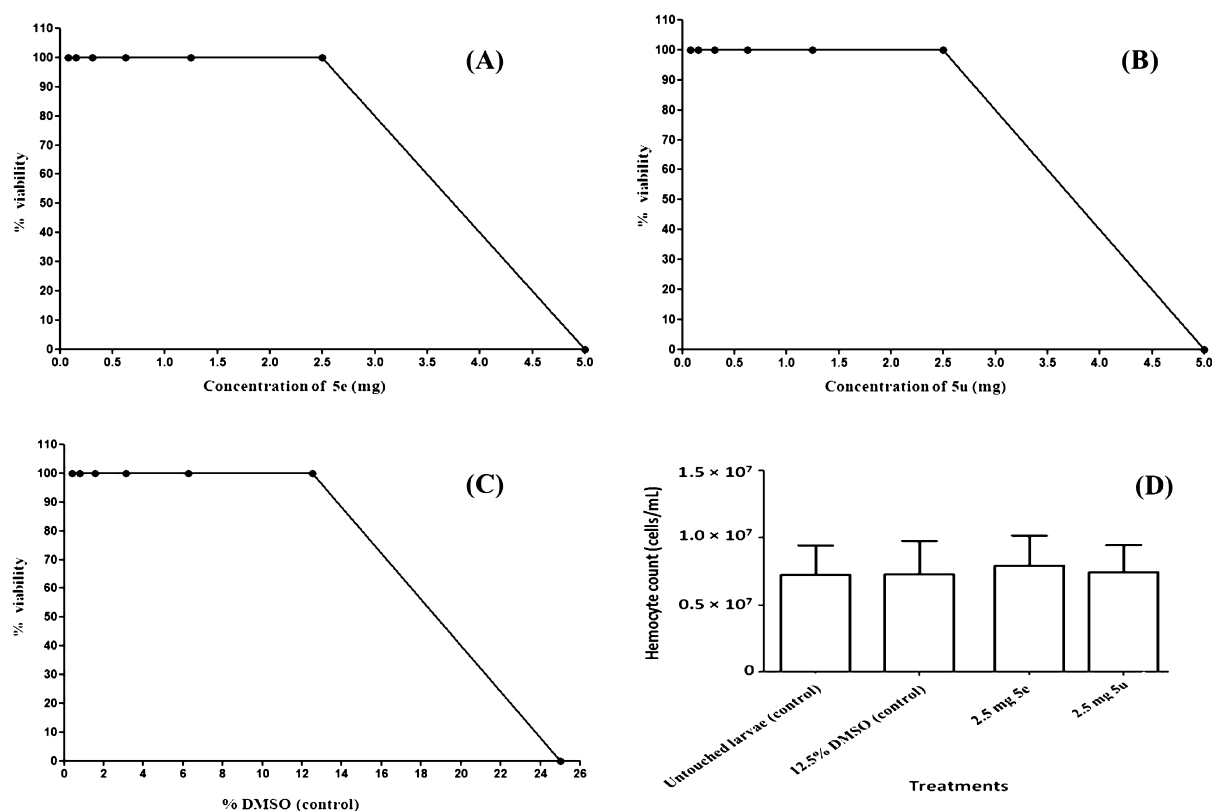


Figure 11. Percentage viability of *G. mellonella* larvae in the presence of (A) **5e**; (B) **5u**; (C) dimethyl sulfoxide (DMSO); (D) hemocyte densities of larvae.

reported in cm^{-1} . ^1H and ^{13}C NMR spectra were obtained in $\text{CDCl}_3/\text{DMSO}-d_6$ as a solvent with tetramethylsilane as an internal standard on a Bruker SpectroSpin DPX-300 spectrometer at 300 and 75 MHz, respectively. Splitting patterns are designated as follows: s (singlet), d (doublet), t (triplet), m (multiplet), sep (septet), or br s (broad). ^1H NMR chemical shift (δ) values are reported in parts per million (ppm) relative to residual solvent (CDCl_3 , δ 7.26; $\text{DMSO}-d_6$, δ 2.54), ^{13}C NMR chemical shifts (δ) are reported in ppm relative to CDCl_3 (δ 77.16; $\text{DMSO}-d_6$, δ 39.5), and coupling constants (J) are expressed in hertz (Hz). Mass spectra were recorded on an Agilent Quadrupole-6150 LC-MS spectrometer. Melting points were measured on a digital Buchi melting point apparatus (M-560) and are uncorrected. Purity was determined by an Agilent RRLC MS 6320 ion trap spectrometer using an XBridge C18 1.7 μm column (50 mm \times 2.1 mm). Mobile phase channel A consisted of 5 mM

ammonium acetate in water. Mobile phase B consisted of acetonitrile with a flow rate = 0.8 mL/min; detection was done by UV@214 nm, and all final compounds were confirmed to have $\geq 95\%$ purity. Purification of the compounds was carried out by silica gel column chromatography (230–400 mesh size) with the indicated eluent.

4.2. General Procedure for the Synthesis of Alkynes (2a–c). A solution of natural precursors (**1a–c**) (1.0 mmol) in anhyd dimethylformamide (10 mL) and potassium carbonate (2.0 mmol) was allowed to stir for 15 min at room temperature. To this solution, propargyl bromide (1.2 mmol) was added dropwise, and the reaction mixture was stirred overnight under argon. After completion of the reaction, the reaction mixture was quenched by the addition of water and extracted with ethyl acetate. The combined organic layers were washed with brine, dried over anhyd sodium sulfate, and concentrated under vacuo. The crude product was then

purified by column chromatography using ethyl acetate/hexane (3:7) to yield the pure alkyne.²⁶

4.2.1. 4-Isopropyl-1-methyl-2-(prop-2-ynyl)benzene (2a). Colorless oil, yield: 87%, $R_f = 0.75$ (ethyl acetate/hexane = 30:70); $^1\text{H NMR}$ (300 MHz, CDCl_3) (δ , ppm): 7.05 (d, $J = 7.5$ Hz, 1H), 6.81–6.76 (m, 2H), 4.69 (s, 2H), 2.87 (sep, $J = 6.9$ Hz, 1H), 2.48 (t, 1H), 2.20 (s, 3H), 1.24 (d, $J = 6.9$ Hz, 6H); $^{13}\text{C NMR}$ (75 MHz, CDCl_3) (δ , ppm): 155.83, 147.85, 130.74, 124.61, 119.17, 110.45, 79.22, 75.17, 56.07, 34.13, 24.12, 15.87; ESI-MS (m/z): 189.2 [$\text{M} + \text{H}$]⁺.

4.2.2. 8-(Prop-2-ynyl)quinoline (2b). Yellow oil, yield: 89%, $R_f = 0.48$ (ethyl acetate/hexane = 30:70); $^1\text{H NMR}$ (300 MHz, CDCl_3) (δ , ppm): 8.95–8.94 (m, 1H), 8.15 (dd, $J = 8.1$, 1.2 Hz, 1H), 8.01 (s, 1H), 7.52–7.42 (m, 2H), 7.29–7.26 (m, 1H), 5.04 (s, 2H), 2.54 (s, 1H); $^{13}\text{C NMR}$ (75 MHz, CDCl_3) (δ , ppm): 162.46, 153.07, 149.38, 135.88, 129.46, 126.39, 121.66, 120.99, 110.05, 78.29, 76.05, 56.51; ESI-MS (m/z): 184.1 [$\text{M} + \text{H}$]⁺.

4.2.3. 2-(Prop-2-ynyl)naphthalene-1,4-dione (2c). Reddish-orange solid, yield: 58%, mp 154–156 °C, $R_f = 0.71$ (ethyl acetate/hexane = 30:70); $^1\text{H NMR}$ (300 MHz, CDCl_3) (δ , ppm): 8.11–8.08 (m, 2H), 7.79–7.70 (m, 2H), 6.36 (s, 1H), 4.81 (s, 2H), 2.66 (s, 1H); $^{13}\text{C NMR}$ (75 MHz, CDCl_3) (δ , ppm): 184.66, 179.77, 158.06, 134.34, 133.44, 131.89, 131.07, 126.72, 126.21, 111.65, 78.17, 75.47, 56.73; ESI-MS (m/z): 145.1.

4.3. General Procedure for the Synthesis of Azides (4a–h). To a solution of substituted aniline (3.22 mmol) in ethyl acetate (6.44 mL) kept at 0 °C was added conc hydrochloric acid (1.29 mL) followed by dropwise addition of a solution of NaNO_2 (3.87 mmol) in water (4.03 mL) over a period of 10 min with constant stirring. After stirring the reaction mixture for 1 h at 0 °C, a solution of NaN_3 (3.87 mmol) in water (4.03 mL) was added to this mixture and allowed to stir at room temperature for 3 h. After completion of the reaction, the mixture was poured into water, extracted with ethyl acetate, dried over anhyd sodium sulfate, and concentrated under vacuo to give azide, which was used further without purification.²⁶

4.4. General Procedure for the Synthesis of 1,2,3-Triazole of Natural Precursors (5a–x). To a solution of substituted aryl azide (1.06 mmol) and alkyne (1.06 mmol) in a mixed solvent system, THF/ H_2O (1:2, 9 mL), were added sodium ascorbate (0.55 mmol) and $\text{CuSO}_4 \cdot 5\text{H}_2\text{O}$ (0.18 mmol). The reaction mixture was stirred overnight at room temperature. After completion of the reaction, the solid obtained was filtered and washed with water. The crude product was purified by silica gel chromatography using a solution of ethyl acetate/hexane (1:9), ethyl acetate/hexane (3:7), and ethyl acetate/hexane (5:5) to yield pure triazole derivatives of carvacrol, 2-hydroxynaphthoquinone, and 8-hydroxyquinoline, respectively.²⁶

4.4.1. 4-((5-Isopropyl-2-methylphenoxy)methyl)-1-phenyl-1H-1,2,3-triazole (5a). Creamish solid, yield: 90%, mp 106–108 °C, $R_f = 0.60$ (ethyl acetate/hexane = 30:70); $^1\text{H NMR}$ (300 MHz, CDCl_3) (δ , ppm): 8.03 (s, 1H), 7.74 (d, $J = 7.8$ Hz, 2H), 7.55–7.42 (m, 3H), 7.08 (d, $J = 7.5$ Hz, 1H), 6.88 (s, 1H), 6.78 (d, $J = 7.2$ Hz, 1H), 5.32 (s, 2H), 2.87 (sep, $J = 6.9$ Hz, 1H), 2.23 (s, 3H), 1.25 (d, $J = 6.9$ Hz, 6H); $^{13}\text{C NMR}$ (75 MHz, CDCl_3) (δ , ppm): 156.32, 148.12, 145.68, 137.07, 130.66, 129.78, 128.84, 124.27, 120.64, 118.86, 110.13, 62.39, 34.11, 24.13, 15.94; ESI-MS (m/z): 308.2 [$\text{M} + \text{H}$]⁺, 330.7 [$\text{M} + \text{Na}$]⁺.

4.4.2. 1-(4-Fluorophenyl)-4-((5-isopropyl-2-methylphenoxy)methyl)-1H-1,2,3-triazole (5b). Creamish solid, yield: 88%, mp 110–113 °C, $R_f = 0.63$ (ethyl acetate/hexane = 30:70); $^1\text{H NMR}$ (300 MHz, CDCl_3) (δ , ppm): 7.98 (s, 1H), 7.74–7.69 (m, 2H), 7.26–7.18 (m, 2H), 7.08 (d, $J = 7.5$ Hz, 1H), 6.87 (s, 1H), 6.79 (d, $J = 7.5$ Hz, 1H), 5.31 (s, 2H), 2.87 (sep, $J = 6.9$ Hz, 1H), 2.22 (s, 3H), 1.25 (d, $J = 6.9$ Hz, 6H); $^{13}\text{C NMR}$ (75 MHz, CDCl_3) (δ , ppm): 164.14, 160.84, 156.28, 148.14, 145.84, 133.33, 130.67, 124.25, 122.68, 122.57, 120.74, 118.90, 116.90, 116.59, 110.11, 62.34, 34.09, 24.11, 15.91; ESI-MS (m/z): 326.2 [$\text{M} + \text{H}$]⁺.

4.4.3. 1-(4-Chlorophenyl)-4-((5-isopropyl-2-methylphenoxy)methyl)-1H-1,2,3-triazole (5c). Creamish solid, yield: 91%, mp 116–118 °C, $R_f = 0.57$ (ethyl acetate/hexane = 30:70); $^1\text{H NMR}$ (300 MHz, CDCl_3) (δ , ppm): 8.00 (s, 1H), 7.70 (d, $J = 8.1$ Hz, 2H), 7.51 (d, $J = 8.4$ Hz, 2H), 7.08 (d, $J = 7.2$ Hz, 1H), 6.87 (s, 1H), 6.79 (d, $J = 7.2$ Hz, 1H), 5.32 (s, 2H), 2.88 (sep, $J = 7.2$ Hz, 1H), 2.22 (s, 3H), 1.24 (d, $J = 6.6$ Hz, 6H); $^{13}\text{C NMR}$ (75 MHz, CDCl_3) (δ , ppm): 156.26, 148.14, 145.97, 135.54, 134.64, 130.68, 129.96, 124.25, 121.76, 120.45, 118.94, 110.13, 62.32, 34.09, 24.11, 15.90; ESI-MS (m/z): 342.1 [$\text{M} + \text{H}$]⁺.

4.4.4. 4-((5-Isopropyl-2-methylphenoxy)methyl)-1-(4-nitrophenyl)-1H-1,2,3-triazole (5d). Light yellow solid, yield: 87%, mp 114–116 °C, $R_f = 0.70$ (ethyl acetate/hexane = 30:70); $^1\text{H NMR}$ (300 MHz, CDCl_3) (δ , ppm): 8.42 (d, $J = 5.1$ Hz, 2H), 8.15 (s, 1H), 7.99 (d, $J = 5.4$ Hz, 2H), 7.09 (d, $J = 7.5$ Hz, 1H), 6.86 (s, 1H), 6.80 (d, $J = 7.8$ Hz, 1H), 5.34 (s, 2H), 2.88 (sep, $J = 6.9$ Hz, 1H), 2.23 (s, 3H), 1.25 (d, $J = 6.9$ Hz, 6H); $^{13}\text{C NMR}$ (75 MHz, CDCl_3) (δ , ppm): 156.13, 148.20, 147.30, 146.71, 141.15, 130.76, 125.55, 124.22, 120.55, 120.36, 119.09, 110.06, 62.18, 34.09, 24.10, 15.90; ESI-MS (m/z): 353.3 [$\text{M} + \text{H}$]⁺.

4.4.5. 4-(4-((5-Isopropyl-2-methylphenoxy)methyl)-1H-1,2,3-triazol-1-yl)benzoic Acid (5e). Creamish solid, yield: 86%, mp 193–196 °C, $R_f = 0.06$ (ethyl acetate/hexane = 30:70); $^1\text{H NMR}$ (300 MHz, CDCl_3) (δ , ppm): 8.30 (d, $J = 8.4$ Hz, 2H), 8.13 (s, 1H), 7.92 (d, $J = 8.4$ Hz, 2H), 7.09 (d, $J = 7.5$ Hz, 1H), 6.88 (s, 1H), 6.80 (d, $J = 7.5$ Hz, 1H), 5.35 (s, 2H), 2.93–2.84 (m, 1H), 2.24 (s, 3H), 1.25 (d, $J = 7.2$ Hz, 6H); $^{13}\text{C NMR}$ (75 MHz, CDCl_3) (δ , ppm): 166.90, 156.49, 153.99, 151.43, 147.97, 145.26, 139.94, 131.57, 130.72, 123.77, 123.13, 120.32, 118.79, 110.84, 61.73, 33.89, 24.41, 16.16; ESI-MS (m/z): 352.1 [$\text{M} + \text{H}$]⁺.

4.4.6. 4-((5-Isopropyl-2-methylphenoxy)methyl)-1-(4-methylphenyl)-1H-1,2,3-triazole (5f). Off-white solid, yield: 88%, mp 90–92 °C, $R_f = 0.71$ (ethyl acetate/hexane = 30:70); $^1\text{H NMR}$ (300 MHz, CDCl_3) (δ , ppm): 7.98 (s, 1H), 7.61 (d, $J = 8.4$ Hz, 2H), 7.31 (d, $J = 8.1$ Hz, 2H), 7.08 (d, $J = 7.5$ Hz, 1H), 6.88 (s, 1H), 6.78 (d, $J = 7.5$ Hz, 1H), 5.31 (s, 2H), 2.88 (sep, $J = 6.9$ Hz, 1H), 2.42 (s, 3H), 2.22 (s, 3H), 1.24 (d, $J = 6.9$ Hz, 6H); $^{13}\text{C NMR}$ (75 MHz, CDCl_3) (δ , ppm): 156.36, 148.10, 145.50, 138.95, 134.80, 130.64, 130.25, 124.28, 120.60, 120.54, 118.83, 110.17, 62.43, 34.10, 24.12, 21.10, 15.92; ESI-MS (m/z): 322.3 [$\text{M} + \text{H}$]⁺.

4.4.7. 4-((5-Isopropyl-2-methylphenoxy)methyl)-1-(4-methoxyphenyl)-1H-1,2,3-triazole (5g). Off-white solid, yield: 90%, mp 83–85 °C, $R_f = 0.48$ (ethyl acetate/hexane = 30:70); $^1\text{H NMR}$ (300 MHz, CDCl_3) (δ , ppm): 7.94 (s, 1H), 7.63 (d, $J = 8.7$ Hz, 2H), 7.09–7.00 (m, 3H), 6.88 (s, 1H), 6.78 (d, $J = 7.5$ Hz, 1H), 5.31 (s, 2H), 3.86 (s, 3H), 2.88 (sep, $J = 6.9$ Hz, 1H), 2.22 (s, 3H), 1.24 (d, $J = 6.9$ Hz, 6H); $^{13}\text{C NMR}$ (75 MHz, CDCl_3) (δ , ppm): 159.89, 156.36, 148.10, 145.43,

130.63, 130.53, 124.27, 122.28, 120.78, 118.82, 114.79, 110.16, 62.43, 55.64, 34.10, 24.12, 15.93; ESI-MS (m/z): 338.2 [M + H]⁺.

4.4.8. 4-(4-((5-Isopropyl-2-methylphenoxy)methyl)-1H-1,2,3-triazol-1-yl)benzenesulfonamide (5h). Creamish solid, yield: 89%, mp 191–193 °C, R_f = 0.38 (ethyl acetate/hexane = 30:70); ¹H NMR (300 MHz, CDCl₃) (δ , ppm): 8.32 (s, 1H), 8.11 (d, J = 8.7 Hz, 2H), 7.94 (d, J = 8.7 Hz, 2H), 7.07 (d, J = 7.5 Hz, 1H), 6.97–6.89 (m, 3H), 6.78 (d, J = 7.8 Hz, 1H), 5.30 (s, 2H), 2.94–2.85 (m, 1H), 2.21 (s, 3H), 1.25 (d, J = 6.9 Hz, 6H); ¹³C NMR (75 MHz, CDCl₃) (δ , ppm): 155.74, 147.51, 145.31, 143.36, 138.59, 130.13, 127.51, 123.66, 120.49, 119.84, 118.40, 109.66, 61.57, 33.49, 23.60, 15.39; ESI-MS (m/z): 387.2 [M + H]⁺.

4.4.9. 8-((1-Phenyl-1H-1,2,3-triazol-4-yl)methoxy)quinoline (5i). Light brown solid, yield: 85%, mp 185–187 °C, R_f = 0.31 (ethyl acetate/hexane = 30:70); ¹H NMR (300 MHz, DMSO-*d*₆) (δ , ppm): 8.99 (s, 1H), 8.03–7.95 (m, 4H), 7.90–7.81 (m, 3H), 7.46 (t, J = 8.6 Hz, 3H), 6.66 (s, 1H), 5.36 (s, 2H); ¹³C NMR (75 MHz, DMSO-*d*₆) (δ , ppm): 154.29, 149.49, 144.25, 140.26, 137.07, 136.30, 130.39, 129.58, 129.25, 127.23, 123.70, 122.36, 120.67, 110.78, 62.29; ESI-MS (m/z): 303.1 [M + H]⁺.

4.4.10. 8-((1-(4-Fluorophenyl)-1H-1,2,3-triazol-4-yl)methoxy)quinoline (5j). Light brown solid, yield: 81%, mp 163–165 °C, R_f = 0.23 (ethyl acetate/hexane = 30:70); ¹H NMR (300 MHz, DMSO-*d*₆) (δ , ppm): 9.01 (s, 1H), 8.82 (br s, 1H), 8.33 (d, J = 8.4 Hz, 1H), 8.01–7.96 (m, 2H), 7.56–7.45 (m, 6H), 5.45 (s, 2H); ¹³C NMR (75 MHz, DMSO-*d*₆) (δ , ppm): 162.94, 154.32, 149.49, 144.29, 136.29, 133.62, 127.23, 123.93, 123.14, 123.02, 120.73, 117.38, 117.08, 110.81, 62.28; ESI-MS (m/z): 321.1 [M + H]⁺.

4.4.11. 8-((1-(4-Chlorophenyl)-1H-1,2,3-triazol-4-yl)methoxy)quinoline (5k). Light brown solid, yield: 82%, mp 129–131 °C, R_f = 0.24 (ethyl acetate/hexane = 30:70); ¹H NMR (300 MHz, DMSO-*d*₆) (δ , ppm): 9.05 (s, 1H), 8.84–8.83 (m, 1H), 8.32 (d, J = 8.1 Hz, 1H), 7.98 (d, J = 8.7 Hz, 2H), 7.68 (d, J = 8.7 Hz, 2H), 7.55–7.52 (m, 3H), 7.46–7.44 (m, 1H), 5.46 (s, 2H); ¹³C NMR (75 MHz, DMSO-*d*₆) (δ , ppm): 154.27, 149.49, 144.44, 140.27, 136.29, 135.85, 133.54, 130.34, 129.59, 127.21, 123.75, 122.35, 120.74, 110.82, 62.28; ESI-MS (m/z): 337.0 [M + H]⁺.

4.4.12. 8-((1-(4-Nitrophenyl)-1H-1,2,3-triazol-4-yl)methoxy)quinoline (5l). Brown solid, yield: 82%, mp 123–125 °C, R_f = 0.21 (ethyl acetate/hexane = 30:70); ¹H NMR (300 MHz, DMSO-*d*₆) (δ , ppm): 9.06 (s, 1H), 8.84 (br s, 1H), 8.33 (d, J = 8.4 Hz, 1H), 7.99 (d, J = 8.7 Hz, 2H), 7.69 (d, J = 8.7 Hz, 2H), 7.56–7.52 (m, 3H), 7.47–7.44 (m, 1H), 5.46 (s, 2H); ¹³C NMR (75 MHz, DMSO-*d*₆) (δ , ppm): 155.42, 149.28, 148.75, 144.26, 140.89, 136.47, 135.42, 133.78, 130.71, 129.32, 127.28, 123.56, 122.48, 120.87, 110.56, 62.36; ESI-MS (m/z): 337.2 [M + H]⁺.

4.4.13. 4-(4-((Quinolin-8-yloxy)methyl)-1H-1,2,3-triazol-1-yl)benzoic Acid (5m). Light brown solid, yield: 83%, mp 276–278 °C, R_f = 0.07 (ethyl acetate/hexane = 30:70); ¹H NMR (300 MHz, DMSO-*d*₆) (δ , ppm): 9.13 (s, 1H), 8.84 (m, 1H), 8.34–8.32 (m, 1H), 8.13–8.10 (m, 4H), 7.56–7.47 (m, 4H), 5.48 (s, 2H); ¹³C NMR (75 MHz, DMSO-*d*₆) (δ , ppm): 169.73, 155.58, 149.78, 148.19, 144.28, 140.67, 136.47, 135.69, 133.42, 130.47, 129.82, 127.47, 123.62, 122.56, 120.86, 110.70, 62.47; ESI-MS (m/z): 347.1 [M + H]⁺.

4.4.14. 8-((1-(4-Methylphenyl)-1H-1,2,3-triazol-4-yl)methoxy)quinoline (5n). Yellowish-brown solid, yield: 80%,

mp 111–113 °C, R_f = 0.25 (ethyl acetate/hexane = 30:70); ¹H NMR (300 MHz, DMSO-*d*₆) (δ , ppm): 8.95 (s, 1H), 8.84 (s, 1H), 8.31 (d, J = 8.1 Hz, 1H), 7.80 (d, J = 8.1 Hz, 2H), 7.55–7.38 (m, 6H), 5.45 (s, 2H), 2.08 (s, 3H); ¹³C NMR (75 MHz, DMSO-*d*₆) (δ , ppm): 154.31, 149.47, 144.13, 140.27, 138.88, 136.30, 134.84, 130.71, 129.59, 127.22, 123.54, 122.34, 120.68, 120.54, 110.77, 62.32, 21.02; ESI-MS (m/z): 317.3 [M + H]⁺.

4.4.15. 8-((1-(4-Methoxyphenyl)-1H-1,2,3-triazol-4-yl)methoxy)quinoline (5o). Light brown solid, yield: 82%, mp 146–148 °C, R_f = 0.19 (ethyl acetate/hexane = 30:70); ¹H NMR (300 MHz, DMSO-*d*₆) (δ , ppm): 8.90 (s, 1H), 8.85–8.83 (m, 1H), 8.32 (dd, J = 8.1, 1.5 Hz, 1H), 7.83 (d, J = 8.7 Hz, 2H), 7.55–7.52 (m, 3H), 7.47–7.44 (m, 1H), 7.14 (d, J = 9.0 Hz, 2H), 5.44 (s, 2H), 3.84 (s, 3H); ¹³C NMR (75 MHz, DMSO-*d*₆) (δ , ppm): 159.82, 154.31, 149.48, 143.99, 140.25, 136.29, 130.48, 129.58, 127.23, 123.65, 122.34, 120.66, 115.37, 110.70, 62.30, 56.03; ESI-MS (m/z): 333.1 [M + H]⁺.

4.4.16. 4-(4-((Quinolin-8-yloxy)methyl)-1H-1,2,3-triazol-1-yl)benzenesulfonamide (5p). Light brown solid, yield: 78%, mp 241–243 °C, R_f = 0.23 (ethyl acetate/hexane = 30:70); ¹H NMR (300 MHz, DMSO-*d*₆) (δ , ppm): 9.13 (s, 1H), 8.34–8.32 (m, 1H), 8.18–8.15 (m, 2H), 8.06–8.03 (m, 2H), 7.54–7.48 (m, 5H), 5.49 (s, 2H); ¹³C NMR (75 MHz, DMSO-*d*₆) (δ , ppm): 159.79, 154.15, 149.32, 144.65, 144.41, 139.03, 136.26, 130.23, 128.01, 127.26, 123.89, 122.45, 120.91, 115.23, 110.81, 62.27; ESI-MS (m/z): 382.1 [M + H]⁺.

4.4.17. 2-((1-Phenyl-1H-1,2,3-triazol-4-yl)methoxy)naphthalene-1,4-dione (5q). Yellow solid, yield: 85%, mp 171–173 °C, R_f = 0.2 (ethyl acetate/hexane = 30:70); ¹H NMR (300 MHz, DMSO-*d*₆) (δ , ppm): 9.03 (s, 1H), 8.30–7.83 (m, 5H), 7.65–7.50 (m, 4H), 6.68 (s, 1H), 5.37 (s, 2H); ¹³C NMR (75 MHz, DMSO-*d*₆) (δ , ppm): 184.96, 179.90, 159.34, 142.44, 136.96, 134.96, 134.11, 131.97, 131.31, 130.38, 129.37, 126.56, 126.02, 124.17, 120.77, 111.50, 62.72; ESI-MS (m/z): 332.2 [M + H]⁺.

4.4.18. 2-((1-(4-Fluorophenyl)-1H-1,2,3-triazol-4-yl)methoxy)naphthalene-1,4-dione (5r). Light brown solid, yield: 82%, mp 242–244 °C, R_f = 0.28 (ethyl acetate/hexane = 30:70); ¹H NMR (300 MHz, DMSO-*d*₆) (δ , ppm): 9.03 (s, 1H), 8.84 (br s, 1H), 8.32 (d, J = 8.1 Hz, 1H), 7.94 (d, J = 8.1 Hz, 2H), 7.61 (d, J = 7.6 Hz, 2H), 7.56–7.44 (m, 3H), 5.46 (s, 2H); ¹³C NMR (75 MHz, DMSO-*d*₆) (δ , ppm): 184.98, 179.92, 159.34, 142.45, 134.99, 134.15, 133.49, 131.96, 131.30, 126.58, 126.04, 124.47, 123.26, 117.39, 117.08, 111.52, 62.68; ESI-MS (m/z): 349.8 [M + H]⁺, 372.2 [M + Na]⁺.

4.4.19. 2-((1-(4-Chlorophenyl)-1H-1,2,3-triazol-4-yl)methoxy)naphthalene-1,4-dione (5s). Light yellow solid, yield: 87%, mp 231–233 °C, R_f = 0.31 (ethyl acetate/hexane = 30:70); ¹H NMR (300 MHz, DMSO-*d*₆) (δ , ppm): 9.04 (s, 1H), 7.98–7.70 (m, 8H), 6.66 (s, 1H), 5.36 (s, 2H); ¹³C NMR (75 MHz, DMSO-*d*₆) (δ , ppm): 184.99, 179.83, 159.32, 142.60, 135.00, 134.15, 133.69, 131.96, 131.31, 130.36, 126.58, 126.04, 124.27, 122.49, 111.51, 62.63; ESI-MS (m/z): 366.0 [M + H]⁺, 388.1 [M + Na]⁺.

4.4.20. 2-((1-(4-Nitrophenyl)-1H-1,2,3-triazol-4-yl)methoxy)naphthalene-1,4-dione (5t). Light yellow solid, yield: 83%, mp 244–247 °C, R_f = 0.23 (ethyl acetate/hexane = 30:70); ¹H NMR (300 MHz, DMSO-*d*₆) (δ , ppm): 9.21 (s, 1H), 8.46 (d, J = 9.0 Hz, 2H), 8.24 (d, J = 9.0 Hz, 2H), 8.02–7.96 (m, 2H), 7.89–7.80 (m, 2H), 6.66 (s, 1H), 5.39 (s, 2H); ¹³C NMR (75 MHz, DMSO-*d*₆) (δ , ppm): 184.95, 179.86, 159.27, 147.35, 143.08, 141.16, 134.98, 134.14, 131.94, 131.28,

126.56, 126.01, 124.58, 121.34, 111.58, 62.54; ESI-MS (m/z): 377.1 [M + H]⁺.

4.4.21. 4-(4-((1,4-Dioxo-1,4-dihydronaphthalen-2-yloxy)methyl)-1H-1,2,3-triazol-1-yl)benzoic Acid (5u). Brown solid, yield: 88%, mp 260–263 °C, R_f = 0.07 (ethyl acetate/hexane = 30:70); ¹H NMR (300 MHz, DMSO- d_6) (δ , ppm): 9.12 (s, 1H), 8.10–7.96 (m, 6H), 7.85–7.81 (m, 2H), 6.65 (s, 1H), 5.36 (s, 2H); ¹³C NMR (75 MHz, DMSO- d_6) (δ , ppm): 184.98, 179.89, 159.30, 142.79, 139.83, 134.98, 134.13, 131.95, 131.29, 126.57, 126.03, 124.27, 120.76, 111.51, 62.60; ESI-MS (m/z): 376.2 [M + H]⁺.

4.4.22. 2-((1-(4-Methylphenyl)-1H-1,2,3-triazol-4-yl)methoxy)naphthalene-1,4-dione (5v). Dark orange solid, yield: 85%, mp 186–188 °C, R_f = 0.20 (ethyl acetate/hexane = 30:70); ¹H NMR (300 MHz, DMSO- d_6) (δ , ppm): 8.95 (s, 1H), 8.01 (t, J = 7.8 Hz, 2H), 7.88–7.78 (m, 4H), 7.41 (d, J = 8.1 Hz, 2H), 6.66 (s, 1H), 5.35 (s, 2H), 2.39 (s, 3H); ¹³C NMR (75 MHz, DMSO- d_6) (δ , ppm): 184.98, 179.91, 159.34, 142.32, 139.04, 134.97, 134.71, 134.13, 131.95, 131.29, 130.73, 126.58, 126.03, 124.06, 120.62, 111.47, 62.73, 21.05; ESI-MS (m/z): 346.2 [M + H]⁺.

4.4.23. 2-((1-(4-Methoxyphenyl)-1H-1,2,3-triazol-4-yl)methoxy)naphthalene-1,4-dione (5w). Light brown solid, yield: 87%, mp 204–206 °C, R_f = 0.22 (ethyl acetate/hexane = 30:70); ¹H NMR (300 MHz, DMSO- d_6) (δ , ppm): 8.91 (s, 1H), 8.01–7.98 (m, 2H), 7.88–7.81 (m, 4H), 7.15 (d, J = 9.0 Hz, 2H), 6.67 (s, 1H), 5.34 (s, 2H), 3.84 (s, 3H); ¹³C NMR (75 MHz, DMSO- d_6) (δ , ppm): 184.97, 179.56, 159.40, 147.63, 143.30, 141.74, 134.54, 134.23, 131.74, 131.21, 126.87, 126.28, 124.75, 121.47, 111.37, 62.85, 55.47; ESI-MS (m/z): 362.2 [M + H]⁺.

4.4.24. 4-(4-((1,4-Dioxo-1,4-dihydronaphthalen-2-yloxy)methyl)-1H-1,2,3-triazol-1-yl) Benzene Sulfonamide (5x). Light brown solid, yield: 85%, mp 204–206 °C, R_f = 0.25; ¹H NMR (300 MHz, DMSO- d_6) (δ , ppm): 9.14 (s, 1H), 8.17 (d, J = 8.4 Hz, 2H), 8.06–7.98 (m, 5H), 7.89–7.72 (m, 2H), 7.56 (s, 2H), 6.67 (s, 1H), 5.39 (s, 2H); ¹³C NMR (75 MHz, DMSO- d_6) (δ , ppm): 184.99, 179.89, 159.30, 144.53, 142.81, 138.93, 134.99, 134.15, 131.95, 131.29, 127.99, 126.58, 126.04, 124.41, 121.05, 111.53, 62.62; ESI-MS (m/z): 362.2 [M + H]⁺.

4.5. General Procedure for the Synthesis of Sulfonic Esters (7a–j). To a solution of natural precursors (1a–b) (1.0 mmol) in dichloromethane (10 mL) was added triethylamine (2.0 mmol) followed by aryl/heteroaryl/aliphatic sulfonyl chloride (6a–e) (1.5 mmol) under an inert atmosphere. The resulting mixture was stirred at room temperature for 3–4 h. After completion of the reaction, water was added and dichloromethane phase was separated, dried over anhydrous sodium sulfate, and evaporated under vacuo. The crude product was purified either by crystallization from ethanol or by column chromatography eluted by using ethyl acetate/hexane (3:7) to yield pure sulfonic esters.²⁷

4.5.1. 5-Isopropyl-2-methylphenyl Benzenesulfonate (7a). Colorless oil, yield: 89%, R_f = 0.33 (ethyl acetate/hexane = 30:70); ¹H NMR (300 MHz, CDCl₃) (δ , ppm): 7.88 (d, J = 7.5 Hz, 2H), 7.68 (t, J = 7.4 Hz, 1H), 7.54 (t, J = 7.5 Hz, 2H), 7.08 (d, J = 7.5 Hz, 1H), 6.99 (d, J = 7.5 Hz, 1H), 6.70 (s, 1H), 2.78 (sep, J = 6.9 Hz, 1H), 2.08 (s, 3H), 1.12 (d, J = 6.6 Hz, 6H); ¹³C NMR (75 MHz, CDCl₃) (δ , ppm): 148.26, 148.07, 136.26, 134.08, 131.35, 129.12, 128.70, 128.51, 125.23, 120.12, 33.39, 23.72, 15.92; ESI-MS (m/z): 157.0.

4.5.2. 5-Isopropyl-2-methylphenyl 4-Nitrobenzenesulfonate (7b). Crystalline solid, yield: 92%, mp 84–86 °C, R_f = 0.45 (ethyl acetate/hexane = 30:70); ¹H NMR (300 MHz, CDCl₃) (δ , ppm): 8.39 (d, J = 8.7 Hz, 2H), 8.09 (t, J = 7.2 Hz, 2H), 7.12–7.04 (m, 2H), 6.78 (s, 1H), 2.81 (sep, J = 6.9 Hz, 1H), 2.08 (s, 3H), 1.15 (d, J = 6.9 Hz, 6H); ¹³C NMR (75 MHz, CDCl₃) (δ , ppm): 150.97, 148.54, 147.96, 141.94, 131.69, 129.84, 128.30, 125.70, 124.27, 119.88, 33.43, 23.72, 15.93; ESI-MS (m/z): 157.0.

4.5.3. 5-Isopropyl-2-methylphenyl 4-Methylbenzenesulfonate (7c). Colorless oil, yield: 85%, R_f = 0.48 (ethyl acetate/hexane = 30:70); ¹H NMR (300 MHz, CDCl₃) (δ , ppm): 7.74 (d, J = 8.4 Hz, 2H), 7.32 (d, J = 8.1 Hz, 2H), 7.07 (d, J = 7.8 Hz, 1H), 6.99 (d, J = 7.8 Hz, 1H), 6.71 (s, 1H), 2.77 (sep, J = 6.9 Hz, 1H), 2.45 (s, 3H), 2.08 (s, 3H), 1.12 (s, J = 6.9 Hz, 6H); ¹³C NMR (75 MHz, CDCl₃) (δ , ppm): 148.30, 147.99, 145.19, 133.28, 131.27, 129.70, 128.71, 128.54, 125.11, 120.18, 33.39, 23.69, 21.67, 15.95; ESI-MS (m/z): 157.1.

4.5.4. 5-Isopropyl-2-methylphenyl Butane-1-sulfonate (7d). Colorless oil, yield: 87%, R_f = 0.31 (ethyl acetate/hexane = 30:70); ¹H NMR (300 MHz, CDCl₃) (δ , ppm): 7.26–7.05 (m, 3H), 3.30 (t, J = 7.9 Hz, 2H), 2.93–2.84 (m, 1H), 2.31 (s, 3H), 2.05–1.95 (m, 2H), 1.60–1.50 (m, 2H), 1.23 (d, J = 6.9 Hz, 6H), 0.99 (t, J = 7.4 Hz, 3H); ¹³C NMR (75 MHz, CDCl₃) (δ , ppm): 148.46, 147.56, 131.51, 128.35, 125.04, 120.18, 51.04, 33.56, 25.51, 23.85, 21.50, 16.26, 13.47; ESI-MS (m/z): 157.0.

4.5.5. 5-Isopropyl-2-methylphenyl Thiophene-2-sulfonate (7e). Colorless oil, yield: 83%, R_f = 0.47 (ethyl acetate/hexane = 30:70); ¹H NMR (300 MHz, CDCl₃) (δ , ppm): 7.73 (dd, J = 5.1, 1.2 Hz, 1H), 7.62 (dd, J = 3.9, 1.2 Hz, 1H), 7.14–7.09 (m, 2H), 7.02 (dd, J = 7.8, 1.2 Hz, 1H), 6.79 (s, 1H), 2.79 (sep, J = 6.9 Hz, 1H), 2.12 (s, 3H), 1.15 (d, J = 6.9 Hz, 6H); ¹³C NMR (75 MHz, CDCl₃) (δ , ppm): 148.35, 148.18, 135.73, 135.09, 134.33, 131.37, 128.73, 127.54, 125.40, 119.92, 33.42, 23.74, 15.83; ESI-MS (m/z): 133.0.

4.5.6. Quinolin-8-yl Benzenesulfonate (7f). Light yellow crystalline solid, yield: 78%, mp 111–113 °C, R_f = 0.19 (ethyl acetate/hexane = 30:70); ¹H NMR (300 MHz, CDCl₃) (δ , ppm): 8.78 (dd, J = 3.9, 1.5 Hz, 1H), 8.14 (dd, J = 8.1, 1.5 Hz, 1H), 7.99 (d, J = 7.5 Hz, 2H), 7.76 (dd, J = 8.1, 0.9 Hz, 1H), 7.63–7.59 (m, 2H), 7.53–7.43 (m, 3H), 7.40–7.36 (m, 1H); ¹³C NMR (75 MHz, CDCl₃) (δ , ppm): 150.86, 145.52, 141.46, 140.95, 135.62, 130.25, 129.35, 128.44, 127.38, 126.41, 123.84, 121.84, 121.31; ESI-MS (m/z): 286.1 [M + H]⁺.

4.5.7. Quinolin-8-yl 4-Nitrobenzenesulfonate (7g). Creamish crystalline solid, yield: 80%, mp 198–200 °C, R_f = 0.34 (ethyl acetate/hexane = 30:70); ¹H NMR (300 MHz, CDCl₃) (δ , ppm): 8.69 (dd, J = 3.9, 1.5 Hz, 1H), 8.32 (d, J = 8.7 Hz, 2H), 8.23–8.17 (m, 3H), 7.83 (d, J = 8.1 Hz, 1H), 7.69 (d, J = 6.9 Hz, 1H), 7.57 (t, J = 7.8 Hz, 1H), 7.44–7.40 (m, 1H); ¹³C NMR (75 MHz, CDCl₃) (δ , ppm): 150.65, 144.89, 141.71, 140.81, 135.86, 130.14, 129.58, 127.62, 126.04, 123.72, 122.77, 122.07; ESI-MS (m/z): 331.1 [M + H]⁺.

4.5.8. Quinolin-8-yl 4-Methylbenzenesulfonate (7h). Off-white solid, yield: 75%, mp 115–117 °C, R_f = 0.37 (ethyl acetate/hexane = 30:70); ¹H NMR (300 MHz, CDCl₃) (δ , ppm): 8.81 (dd, J = 4.2, 1.5 Hz, 1H), 8.12 (dd, J = 8.4, 1.8 Hz, 1H), 7.86 (d, J = 8.4 Hz, 2H), 7.73 (dd, J = 8.1, 1.2 Hz, 1H), 7.58 (dd, J = 7.5, 1.2 Hz, 1H), 7.48 (t, J = 7.9 Hz, 1H), 7.40–7.36 (m, 1H), 7.24 (d, J = 8.4 Hz, 2H), 2.39 (s, 3H); ¹³C NMR (75 MHz, CDCl₃) (δ , ppm): 150.78, 145.56, 145.03,

141.60, 135.71, 133.22, 129.62, 129.43, 128.77, 126.97, 125.98, 122.44, 121.84, 21.65; ESI-MS (m/z): 300.1 $[M + H]^+$.

4.5.9. Quinolin-8-yl Butane-1-sulfonate (7i). Colorless oil, yield: 79%, $R_f = 0.47$ (ethyl acetate/hexane = 30:70); 1H NMR (300 MHz, $CDCl_3$) (δ , ppm): 8.97 (dd, $J = 4.2, 1.5$ Hz, 1H), 8.21 (dd, $J = 8.4, 1.5$ Hz, 1H), 7.78 (d, $J = 8.4$ Hz, 1H), 7.73 (d, $J = 7.5$ Hz, 1H), 7.55 (t, $J = 7.8$ Hz, 1H), 7.50–7.46 (m, 1H), 3.62 (t, $J = 7.8$ Hz, 2H), 2.16–2.05 (m, 2H), 1.59–1.47 (m, 2H), 0.98 (t, $J = 7.3$ Hz, 3H); ^{13}C NMR (75 MHz, $CDCl_3$) (δ , ppm): 150.79, 145.52, 141.44, 136.13, 129.73, 126.93, 126.33, 128.55, 122.00, 51.83, 25.51, 21.51, 13.47; ESI-MS (m/z): 266.2 $[M + H]^+$.

4.5.10. Quinolin-8-yl Thiophene-2-sulfonate (7j). Creamish solid, yield: 85%, mp 103–105 °C, $R_f = 0.24$ (ethyl acetate/hexane = 30:70); 1H NMR (300 MHz, $CDCl_3$) (δ , ppm): 8.81 (dd, $J = 4.2, 1.8$ Hz, 1H), 8.14 (dd, $J = 8.4, 1.8$ Hz, 1H), 7.76 (dd, $J = 8.1, 1.2$ Hz, 1H), 7.68 (dd, $J = 3.9, 1.5$ Hz, 1H), 7.65–7.62 (m, 2H), 7.52 (t, $J = 10.2$ Hz, 1H), 7.41–7.37 (m, 1H), 7.01 (t, $J = 4.4$ Hz, 1H); ^{13}C NMR (75 MHz, $CDCl_3$) (δ , ppm): 150.87, 145.55, 141.53, 135.75, 135.50, 135.34, 134.42, 129.58, 127.29, 126.02, 122.72, 121.92; ESI-MS (m/z): 292.0 $[M + H]^+$.

4.6. X-ray Crystallographic Analysis. The structures of compounds **5c**, **5f**, **7g**, and **7h** were unambiguously established by X-ray crystallographic analysis. Single crystals of **5c**, **7g**, and **7h** were obtained through the slow evaporation of their mixed solvent system containing dichloromethane, hexane, methanol, and ethyl acetate, whereas single crystal of **5f** was obtained through the slow evaporation of its ethyl acetate and hexane solution. Suitable crystal of compound **5c** ($C_{19}H_{20}ClN_3O$) was selected and analyzed on a Nonius Kappa charge-coupled device (CCD) diffractometer, and single crystals of compounds **5f** ($C_{20}H_{23}N_3O$) and **7g** ($C_{15}H_{10}N_2O_5S$) were analyzed on a D8 Venture Dual Source 100 CMOS diffractometer (Karlsruhe, Germany) equipped with Cu radiation ($Cu K\alpha = 1.54178 \text{ \AA}$). For analyzing the single crystal of compound **7h** ($C_{16}H_{13}NO_3S$), a Bruker APEX II Kappa CCD diffractometer was utilized. Intensity data were collected at 100 K using ϕ and ω scans. No significant loss in intensities was observed during data collection. Multiscan absorption corrections were applied to the intensity data empirically using Denzo for **5c**²⁸ and SADABS V2014/2²⁹ for **5f**, **7g**, and **7h**. Data collection, reduction, and refinement were performed using COLLECT,³⁰ Denzo-SMN,³¹ and SHELXL-97³² softwares for **5c**, and for **5f**, **7g**, and **7h**, APEX2 V2014.5-0,³³ SAINT V8.34A,³⁴ and SHELXL-2014³⁵ softwares were used, respectively. Crystal structures were solved by direct methods using SHELXL-97³⁶ for **5c** and SHELXT-2014³⁵ for **5f**, **7g**, and **7h** and refined with full-matrix least-squares based on F^2 using SHELXT-2014.³⁵ All nonhydrogen atoms were refined anisotropically. Hydrogen atoms were first located in the Fourier difference map, then positioned geometrically, and allowed to ride on their respective parent atoms. The molecular graphics and crystallographic illustrations were prepared using XP.^{37,38}

4.7. In Vitro Antimicrobial Activity. All synthesized compounds (**5a–x** and **7a–j**) were screened for their in vitro antibacterial activity against *S. pneumoniae* (MTCC 655), *E. faecalis* (MTCC 439), *P. aeruginosa* (MTCC 2453), *S. enterica* (MTCC 3224), *K. pneumoniae* (ATCC 700603), *E. coli* (ATCC 25922), and multidrug-resistant strains viz. *E. coli* MRA11 (GenBank accession no. KJ957160), MRC17 (GenBank accession no. KJ906623), MRC24 (GenBank

accession no. KM822765), MRAE26 (GenBank accession no. KJ923014), MRAE32 (GenBank accession no. KJ923017), MRAE33 (GenBank accession no. KM822768), MRAE44 (GenBank accession no. KJ923018), and MROB11 (GenBank accession no. KC963018) using the broth dilution technique according to the standard protocol for antibacterial assessment by CLSI.³⁹ CIP was used as a positive control for the studies. All compounds were dissolved in DMSO and serially diluted in broth medium to achieve the final concentration of DMSO less than 4%. Varying concentrations (1000 to 7.8 $\mu\text{g/mL}$) of test compounds were dispensed into a 96-well plate in nutrient broth in a final volume of 100 μL . Then, 100 μL of bacterial cells (approximately 2.5×10^6 cells/mL) was dispensed into the 96-well plate (Tarson) and incubated at 37 °C for overnight. After the incubation period, each well was analyzed for the presence or absence of visual growth of bacterial cells. The lowest concentration of the test compound at which no visible growth occurs represents its MIC value. Moreover, after incubation, the growth was measured turbidometrically at 600 nm using a Thermo Multiskan Go spectrophotometer. IC_{50} was determined as 50% inhibition of bacterial cell growth and calculated by plotting a graph between concentration (\log_{10}) and % inhibition. In the case of MDR isolates, varying concentrations (8–1024 $\mu\text{g/mL}$ for **5e** and **5u** and 0.49–63.3 $\mu\text{g/mL}$ for CIP) were dispensed into a 96-well plate (Tarson) in Luria broth medium. Then, the medium was inoculated with 10 μL of 1000 times diluted 0.1OD₆₀₀ culture and incubated overnight at 37 °C. The optical density (OD) was measured at 600 nm using a microplate reader (Thermo Scientific Multiskan Go). Percentage inhibition of these resistant isolates was calculated using the formula

$$\text{Percentage inhibition} = a - b/a \times 100$$

where a = pure culture reading – media reading and b = test reading – plain compound reading (if the compound is a colored solution).

4.8. Synergistic Study. The antimicrobial activity of the test compounds in combination with CIP was determined following the checkerboard method. A 96-well microtiter plate was inoculated with 100 μL of Mueller-Hinton broth followed by addition of compounds **5e** and **5u** with the concentration ranging from 1024 to 16 $\mu\text{g/mL}$ and CIP with the concentration ranging from 128 to 2 $\mu\text{g/mL}$. Each well was inoculated with 100 μL of a suspension of 5×10^5 CFU/mL in a final volume of 200 μL . Inocula were prepared by direct suspension in Mueller-Hinton broth of bacteria grown overnight on MacConkey medium in order to obtain 0.5 McFarland standard. The checkerboard plates were then incubated for overnight at 37 °C. The FICI is defined as the sum of the MICs of each drug when used in combination divided by the MIC of the drug used alone. Synergy and antagonism were defined by $FICI \leq 0.5$ and >4 , respectively. Partially synergistic was denoted by $0.5 > FICI < 1$, whereas indifferent was defined by $1 < FICI \leq 4$.⁴⁰

4.9. Growth Kinetic Studies. The bacterial strains *S. pneumoniae* and *E. coli* were freshly revived by subculturing on the nutrient agar plate. A loop of inoculum was introduced into the nutrient broth medium and incubated in an automated incubator shaker for 12 h at 37 °C. On the second day, approx. 2×10^6 cells/mL of overnight grown culture were inoculated in 50 mL of sterile nutrient broth medium. Different concentrations (2MIC, MIC, and MIC/2) of inhibitors **5e** and **5u** were added into the culture medium and incubated at

37 °C and 160 rpm. CIP at a concentration 10 µg/mL was used as a positive control drug. Aliquots (1 mL) of culture were removed from each test sample at time interval of 2 h (i.e., time points of 0, 2, 4, 6, 8, 10, 12, 14, 16, 18, 20, and 22 h), and growth was measured turbidometrically at 600 nm using a Thermo Multiskan Go spectrophotometer. OD was recorded for each concentration against time (h).⁴¹

4.10. TEM Analysis. The morphology of *S. pneumoniae* and *E. coli* cells was analyzed using TEM following the standard protocol.⁴² Briefly, the cells were harvested, standardized ($A_{600} \approx 0.1$), and exposed to 62.5 and 125 µg/mL concn of test inhibitors **5e** for *E. coli* and *S. pneumoniae*, respectively, and 125 µg/mL of **5u** for both the strains for 1 h. Then, the cells were washed thrice with phosphate-buffered saline (PBS) to remove the residual medium and fixed overnight in 2.5% glutaraldehyde in phosphate/magnesium buffer (40 mM K_2HPO_4/KH_2PO_4 , pH 6.5, 0.5 mM $MgCl_2$). The cells were washed twice for 15 min in 0.1 M sodium phosphate buffer (pH 6.0) and postfixed for 2 h in 2% osmium tetroxide. Again, the cells were washed twice for 15 min in distilled water and then en bloc stained with 1% uranyl acetate (aqueous) for 30 min. After two further washes, cells were dehydrated in 95 and 100% ethanol. The cells were exposed to propylene oxide for 2 × 10 min and infiltrated for 1 h in 1:1 propylene/epoxy embedding material (Epon) mixture and then overnight in fresh Epon. After polymerization for 48 h at 60 °C, ultrathin sections were cut using a microtome (Leica EM UC6) and transferred onto a copper grid. The samples were stained with uranyl acetate (saturated solution of uranyl acetate in 50% alcohol) followed by lead citrate. The samples were washed three times in Milli-Q water and dried by blotting with Whatman filter paper. The sections were examined with a Tecnai G2 20 high-resolution transmission electron microscope (Fei Company, The Netherlands) at 200 kV.

4.11. Assessment of Anti-Biofilm Activity by XTT Assay. A semi-quantitative measurement of metabolic activity of bacterial biofilm was obtained from the XTT (2,3-bis(2-methoxy-4-nitro-5-sulphophenyl)-5-[(phenylamino)carbonyl]-2H-tetrazolium-hydroxide) reduction assay.⁴³ A serial 2-fold dilution pattern was prepared in the medium wells with the concentration of antibacterial agents ranging from 7.812 to 1000 µg/mL. Aliquots of 100 µL of tryptic soy broth (TSB) with a bacterial inoculum of 5×10^5 CFU/mL were added to each well and incubated at 37 °C for 24 h under static conditions. The medium was discarded and washed with PBS to remove the nonadherent bacteria. To each well, 50 µL of prepared XTT salt solution (HiMedia, India) was added and plates were incubated at 37 °C in dark for 90 min. Bacterial dehydrogenase activity reduces XTT tetrazolium salt to XTT formazan, resulting in colorimetric change (turns to orange) that was correlated with cell viability. The colorimetric changes were measured spectrophotometrically at 490 nm.⁴⁴ The % inhibition data were interpreted from dose–response curves.

4.12. Assessment of Anti-Biofilm Activity by Crystal-Violet Assay. Biofilm formation by *E. coli* and *S. pneumoniae* was investigated using crystal violet assay based on the methods of O'Toole & Kolter.⁴⁵ Cultures were grown in TSB (containing 2.5 g/L glucose) until OD_{600} reached 0.1 (equivalent to 0.5 McFarland). The cultures were diluted in fresh TSB medium in a 1:1 ratio (added 100 µL of culture in 100 µL of broth), and polystyrene 96-well microtitre plates were filled with 200 µL of culture per well and incubated at 37 °C for 48 h. After incubation, cultures were removed and

microtitre plate wells were gently washed four times with 200 µL of sterile PBS (1× PBS, pH=7.2) to remove loosely associated bacteria. Cells that had adhered to the wells were stained with 200 µL of 0.1% (w/v) crystal violet at room temperature for 20 min. The wells were washed again with 1× PBS or sterile distilled water. The crystal violet that had stained the cells was solubilized in 250 µL of 95% (v/v) ethanol. The samples were incubated for 20 min at room temperature, and biofilm formation was quantified by measuring the OD at 590 nm in an ELISA plate reader (Thermo Scientific, Multiskan Go). To observe the change in the amount of biofilm formation in the presence of compounds **5e**, **5u**, and CIP at a subinhibitory level, TSB medium was supplemented with 125, 250, and 8 µg/mL, respectively, for *E. coli* and 250, 250, and 8 µg/mL, respectively, for *S. pneumoniae*. The wells containing TSB medium alone were used as blank.

The percentage of biofilm inhibition was calculated by the formula

$$\text{Percentage inhibition} = a - b/a \times 100$$

where a = pure culture reading – media reading and b = test reading – plain compound reading (if the compound is a colored solution).

4.13. Assessment of Biofilm Inhibition by SEM Analysis. SEM analysis was performed to determine the biofilm formation by *E. coli*. The fresh bacterial cultures were prepared and inoculated into six-well cell culture plates containing 3 mL of TSB (containing 2.5 g/L glucose). Glass coverslips (8 mm diam) were dispensed into each well for biofilm formation on the surface and incubated at 37 °C for 24 h. Post incubation, plates were removed and test compounds were added to determine the anti-biofilm effect. Parafilm-sealed plates were further incubated for the next 24 h. Coverslips were removed after total incubation of 24 h and washed with 0.1 M PBS. Biofilms that formed on the coverslips were placed in a fixative (4%, v/v, formaldehyde in PBS) overnight. Samples were again washed with PBS, and then coverslips were left to dry and later examined under a scanning electron microscope.⁴⁶

4.14. Cytotoxicity by MTT Assay. MTT (3-(4,5-Dimethyl-2-yl)-2,5-diphenyl tetrazolium bromide), Dulbecco's modified Eagle's medium (DMEM), 0.25% trypsin, and a 0.02% ethylenediaminetetraacetic acid (EDTA) mixture were purchased from HiMedia (Mumbai, India). Fetal bovine serum (FBS) was obtained from Gibco (Grand Island, NY). The human embryonic kidney (HEK293) cell line was procured from National Centre for Cell Sciences (NCCS), Pune, India. The cells were cultured and maintained as a monolayer in DMEM supplemented with 10% FBS and antibiotics (100 units/mL penicillin and 100 µg/mL streptomycin) at 37 °C in a humidified atmosphere of 5% CO_2 in T-25 flasks. The cells were subcultured twice in a week. A cell count of approximately 2×10^4 cells per well was seeded in a 96-well plate (150 µL per well) and incubated for 24 h before treatment. The cells were then treated with varying concentrations (10–400 µg/mL) of the test compounds. After 48 h of incubation at 37 °C, the exhausted serum-supplemented medium was removed and serum-free medium (50 µL) was added into each well. After that, 20 µL per well of MTT at a concentration of 5 mg/mL in PBS was added to each well and the plates were incubated for 4 h at 37 °C. Formazan crystals, the metabolized MTT product, were solubilized in DMSO (150 µL per well) and were quantified

by reading the absorbance at 570 nm after incubation of 10 min on an *iMark* microplate reader (Bio-Rad, Hercules, CA). All assays were performed in triplicate. Percent viability was taken as the relative absorbance of treated versus untreated control cells.²¹

4.15. Hemolytic Assay. The hemolytic activities of the test inhibitors **5e** and **5u** and the conventional antibacterial drug CIP (HiMedia) were determined on hRBCs.²¹ Human erythrocytes from healthy individuals were collected in tubes containing EDTA as an anticoagulant. The erythrocytes were harvested by centrifugation for 10 min at 2000 rpm and 20 °C and washed three times in PBS. To the pellet, PBS was added to yield a 10% (v/v) erythrocyte/PBS suspension. The 10% suspension of erythrocytes was then further diluted with PBS at a 1:10 ratio. The final diluted erythrocytes (100 μ L) were added to 100 μ L of PBS having a previously determined concentration gradient (1000 to 7.8 μ g/mL) of test compounds in microcentrifuge tubes. Total hemolysis was achieved with 1% Triton X-100. The tubes were incubated for 1 h at 37 °C and then centrifuged for 10 min at 2000 rpm and at room temperature. From the supernatant fluid, 150 μ L was transferred to a flat-bottomed microtitre plate (Tarson), and the absorbance was measured spectrophotometrically at 450 nm by using a Thermo Multiskan Go spectrophotometer. The hemolysis percentage was calculated by following the equation:

$$\% \text{ Hemolysis} = \left[\frac{(A_{450} \text{ of test compound treated sample} - A_{450} \text{ of buffer treated sample})}{(A_{450} \text{ of 1\% Triton X-100 treated sample} - A_{450} \text{ of buffer treated sample})} \right] \times 100\%$$

where A_{450} is absorbance at 450 nm.

4.16. In Vivo Toxicity Evaluation of 5e and 5u in *G. mellonella* Larvae. The larvae of the sixth developmental stage of *G. mellonella* were obtained from the Mealworm Company (Sheffield, England). The larvae of *G. mellonella* were stored in wood shavings in the dark at 15 °C prior to use. The larvae that were chosen for experiments weighed 0.21 g and were used within 3–4 weeks of receipt. Ten healthy larvae were placed in sterile 9 cm Petri dishes with Whatman filter paper inserted inside. A culture of *S. pneumoniae* and *E. coli* was grown to the stationary phase ($1-2 \times 10^8$ /mL) in YEPD broth at 30 °C and 200 rpm. The cells were harvested by centrifugation (2056g for 5 min on a Beckmann GS-6 bench centrifuge), washed in PBS, and resuspended in PBS at a cell density 5×10^5 per 20 μ L. The larvae were inoculated by injecting 20 μ L through the last left proleg into the hemocoel using a Myjector syringe (Terumo Europe) and placed at 30 °C in the dark. One hour post inoculation, the larvae were inoculated with compounds **5e** and **5u**, both at a concentrations of 2.5 mg suspended in PBS, and supplemented with 12.5% DMSO (v/v), through the last right proleg. The larvae injected with 20 μ L of PBS supplemented with 12.5% DMSO (v/v) were used as controls. For assessment of larval viability, the larvae were gently probed with a needle, and if no response was observed, the larvae were considered to be dead.

Three larvae were inoculated with 20 μ L of **5e** and **5u** solutions at a concentration of 1.25 or 2.5 mg/mL. The larvae were then incubated at 30 °C, in the dark, for 24 h. The hemocyte density in the larvae was ascertained by piercing the backs of the anterior end (“head”) of the three larvae with a sterile needle and collecting the yellow hemolymph (“blood”),

ensuring no white floccular material was removed—this is the fat body and will impede counting. Hemolymph was diluted to 1 in 10 in cold PBS containing 0.37% (v/v) 2-mercaptoethanol to reduce clotting and melanization. The solution was mixed gently by pipetting. Hemocytes were counted on a hemocytometer (0.0025 mm², BLAUBRAND, Germany), and the density in the original larvae was calculated.²¹

4.17. ADME Profiling. A computational study to predict ADME properties of the synthesized compounds (**5a–x** and **7a–j**) was performed using QikProp version 3.2, Schrödinger software. Various physicochemical significant descriptors as well as pharmacokinetically relevant properties such as molecular weight, number of hydrogen bond acceptors/donors, NRBs, aqueous solubility, brain/blood partition coefficient, binding to human serum albumin, and % human oral absorption of the compounds were evaluated. In particular, Lipinski’s rule of 5 was compiled for all synthesized compounds, which is widely used as a filter to identify easily bioavailable drugs. Moreover, QikProp provides ranges to compare molecule properties with those of 95% of known drugs.²⁴

■ ASSOCIATED CONTENT

📄 Supporting Information

The Supporting Information is available free of charge on the ACS Publications website at DOI: 10.1021/acsomega.8b00582.

X-ray crystallographic analysis of **5c**, **5f**, **7g**, and **7h**, physicochemical parameters of compounds **5a–x** and **7a–j**, and spectral data for representative compounds (PDF)

■ AUTHOR INFORMATION

Corresponding Author

*E-mail: mabid@jmi.ac.in. Phone: +91-8750295095. Fax: +91-11-26980229 (Mohammad Abid).

ORCID

Umesh Yadava: 0000-0002-9127-532X

Mohammad Abid: 0000-0002-0507-8451

Notes

The authors declare no competing financial interest.

■ ACKNOWLEDGMENTS

Mohammad Abid gratefully acknowledges the University Grant Commission (UGC), Govt. of India, for a RAMAN Postdoctoral Fellowship (F. no. 5-123/2016(IC)) to work at the Eppley Institute, UNMC, Omaha, NE, USA. B.A. acknowledges BSR meritorious fellowship support from UGC.

■ REFERENCES

- (1) Kumar, S. V.; Scottwell, S. Ø.; Waugh, E.; McAdam, C. J.; Hanton, L. R.; Brooks, H. J. L.; Crowley, J. D. Antimicrobial Properties of Tris(homoleptic) Ruthenium(II) 2-Pyridyl-1,2,3-triazole “Click” Complexes against Pathogenic Bacteria, Including Methicillin-Resistant *Staphylococcus aureus* (MRSA). *Inorg. Chem.* **2016**, *55*, 9767–9777.
- (2) Tanino, T.; Ichikawa, S.; Al-Dabbagh, B.; Bouhss, A.; Oyama, H.; Matsuda, A. Synthesis and biological evaluation of muraymycin analogues active against anti-drug-resistant bacteria. *ACS Med. Chem. Lett.* **2010**, *1*, 258–262.
- (3) Natan, M.; Gutman, O.; Lavi, R.; Margel, S.; Banin, E. Killing mechanism of stable *N*-halamine cross-linked polymethacrylamide

nanoparticles that selectively target bacteria. *ACS Nano* **2015**, *9*, 1175–1188.

(4) Bresee, J.; Bond, C. M.; Worthington, R. J.; Smith, C. A.; Gifford, J. C.; Simpson, C. A.; Carter, C. J.; Wang, G.; Hartman, J.; Osbaugh, N. A.; Shoemaker, R. K.; Melander, C.; Feldheim, D. L. Nanoscale Structure-Activity Relationships, Mode of Action, and Biocompatibility of Gold Nanoparticle Antibiotics. *J. Am. Chem. Soc.* **2014**, *136*, 5295–5300.

(5) Frieden, T. Antibiotic resistance threats in the United States. <http://www.cdc.gov/drugresistance/threat-report-2013/index.html>, 2013.

(6) Burt, S. A.; Ojo-Fakunle, V. T. A.; Woertman, J.; Veldhuizen, E. J. A. The natural antimicrobial carvacrol inhibits quorum sensing in *Chromobacterium violaceum* and reduces bacterial biofilm formation at sub-lethal concentrations. *PLoS One* **2014**, *9*, No. e93414.

(7) Bunders, C. A.; Richards, J. J.; Melander, C. Identification of aryl 2-aminoimidazoles as biofilm inhibitors in Gram-negative bacteria. *Bioorg. Med. Chem. Lett.* **2010**, *20*, 3797–3800.

(8) Maher, M. C.; Lim, J. Y.; Gunawan, C.; Cegelski, L. Cell-based high-throughput screening identifies rifapentine as an inhibitor of amyloid and biofilm formation in *Escherichia coli*. *ACS Infect. Dis.* **2015**, *1*, 460–468.

(9) Duong, H. T. T.; Jung, K.; Kutty, S. K.; Agustina, S.; Adnan, N. N. M.; Basuki, J. S.; Kumar, N.; Davis, T. P.; Barraud, N.; Boyer, C. Nanoparticle (star polymer) delivery of nitric oxide effectively negates *Pseudomonas aeruginosa* biofilm formation. *Biomacromolecules* **2014**, *15*, 2583–2589.

(10) Bunders, C.; Cavanagh, J.; Melander, C. Flustramine inspired synthesis and biological evaluation of pyrroloindoline triazole amides as novel inhibitors of bacterial biofilms. *Org. Biomol. Chem.* **2011**, *9*, 5476–5481.

(11) Minvielle, M. J.; Bunders, C. A.; Melander, C. Indole-triazole conjugates are selective inhibitors and inducers of bacterial biofilms. *MedChemComm* **2013**, *4*, 916–919.

(12) Ballard, T. E.; Richards, J. J.; Wolfe, A. L.; Melander, C. Synthesis and Antibiofilm Activity of a Second-Generation Reverse-Amide Oroidin Library: A Structure-Activity Relationship Study. *Chem.—Eur. J.* **2008**, *14*, 10745–10761.

(13) Rogers, S. A.; Melander, C. Construction and Screening of a 2-Aminoimidazole Library Identifies a Small Molecule Capable of Inhibiting and Dispersing Bacterial Biofilms across Order, Class, and Phylum. *Angew. Chem., Int. Ed.* **2008**, *47*, 5229–5231.

(14) Huigens, R. W., III; Rogers, S. A.; Steinhauer, A. T.; Melander, C. Inhibition of *Acinetobacter baumannii*, *Staphylococcus aureus* and *Pseudomonas aeruginosa* biofilm formation with a class of TAGE-triazole conjugates. *Org. Biomol. Chem.* **2009**, *7*, 794–802.

(15) Nagender, P.; Malla Reddy, G.; Naresh Kumar, R.; Poornachandra, Y.; Ganesh Kumar, C.; Narsaiah, B. Synthesis, cytotoxicity, antimicrobial and anti-biofilm activities of novel pyrazolo[3,4-b]pyridine and pyrimidine functionalized 1,2,3-triazole derivatives. *Bioorg. Med. Chem. Lett.* **2014**, *24*, 2905–2908.

(16) Linares, D.; Bottzcek, O.; Pereira, O.; Praud-Tabariès, A.; Blache, Y. Designing 2-aminoimidazole alkaloids analogs with anti-biofilm activities: Structure-activities relationships of polysubstituted triazoles. *Bioorg. Med. Chem. Lett.* **2011**, *21*, 6751–6755.

(17) Praud-Tabariès, A.; Dombrowsky, L.; Bottzcek, O.; Briand, J.-F.; Blache, Y. Synthesis of a polyprenyl-type library containing 1,4-disubstituted-1,2,3-triazoles with anti-biofilm activities against *Pseudoalteromonas* sp. *Tetrahedron Lett.* **2009**, *50*, 1645–1648.

(18) Aneja, B.; Irfan, M.; Hassan, M. I.; Prakash, A.; Yadava, U.; Daniliuc, C. G.; Zafaryab, M.; Rizvi, M. M.; Azam, A.; Abid, M. Monocyclic β -lactam and unexpected oxazinone formation: Synthesis, crystal structure, docking studies and antibacterial evaluation. *J. Enzyme Inhib. Med. Chem.* **2016**, *31*, 834–852.

(19) Masood, M. M.; Pillalamarri, V. K.; Irfan, M.; Aneja, B.; Jairajpuri, M. A.; Zafaryab, M.; Rizvi, M. M. A.; Yadava, U.; Adlagatta, A.; Abid, M. Diketo acids and their amino acid/dipeptidic analogues as promising scaffolds for the development of bacterial

methionine aminopeptidase inhibitors. *RSC Adv.* **2015**, *5*, 34173–34183.

(20) Irfan, M.; Aneja, B.; Yadava, U.; Khan, S. I.; Manzoor, N.; Daniliuc, C. G.; Abid, M. Synthesis, QSAR and anticandidal evaluation of 1,2,3-triazoles derived from naturally bioactive scaffolds. *Eur. J. Med. Chem.* **2015**, *93*, 246–254.

(21) Aneja, B.; Irfan, M.; Kapil, C.; Jairajpuri, M. A.; Maguire, R.; Kavanagh, K.; Rizvi, M. M. A.; Manzoor, N.; Azam, A.; Abid, M. Effect of novel triazole-amino acid hybrids on growth and virulence of *Candida* species: in vitro and in vivo studies. *Org. Biomol. Chem.* **2016**, *14*, 10599–10619.

(22) Fallon, J.; Kelly, J.; Kavanagh, K. *Galleria mellonella* as a model for fungal pathogenicity testing. *Host-Fungus Interactions*; Humana Press, 2012; pp 469–485.

(23) Lin, J.; Sahakian, D.; de Moraes, S.; Xu, J.; Polzer, R.; Winter, S. The role of absorption, distribution, metabolism, excretion and toxicity in drug discovery. *Curr. Top. Med. Chem.* **2003**, *3*, 1125–1154.

(24) *Small-Molecule Drug Discovery Suite 2017-3*; Schrödinger, LLC: New York, NY, 2017.

(25) Lipinski, C. A.; Lombardo, F.; Dominy, B. W.; Feeney, P. J. Experimental and computational approaches to estimate solubility and permeability in drug discovery and development settings. PII of original article: S0169-409X(96)00423-1. The article was originally published in *Advanced Drug Delivery Reviews* **23** (1997) 3-25.1. *Adv. Drug Delivery Rev.* **2001**, *46*, 3–26.

(26) Aneja, B.; Arif, R.; Perwez, A.; Napoleon, J. V.; Hasan, P.; Rizvi, M. M. A.; Azam, A.; Rahisuddin; Abid, M. N-substituted 1,2,3-triazolyl-appended indole-chalcone hybrids as potential DNA intercalators endowed with antioxidant and anticancer properties. *ChemistrySelect* **2018**, *3*, 2638–2645.

(27) Firouzabadi, H.; Iranpoor, N.; Gholinejad, M.; Samadi, A. Copper(I) iodide catalyzes odorless thioarylation of phenolic esters with alkyl derivatives using thiourea in wet polyethylene glycol (PEG 200). *J. Mol. Catal. A: Chem.* **2013**, *377*, 190–196.

(28) Otwinowski, Z.; Borek, D.; Majewski, W.; Minor, W. Multiparametric scaling of diffraction intensities. *Acta Crystallogr., Sect. A: Found. Crystallogr.* **2003**, *59*, 228–234.

(29) SADABS; Bruker AXS Inc.: Madison, WI, USA, 2014.

(30) Hooft, R. W. W. COLLECT; Bruker AXS: Delft, The Netherlands, 2008.

(31) Otwinowski, Z.; Minor, W. [20] Processing of X-ray diffraction data collected in oscillation mode. *Methods Enzymol.* **1997**, *276*, 307–326.

(32) Sheldrick, G. M. A short history of SHELX. *Acta Crystallogr., Sect. A: Found. Crystallogr.* **2008**, *64*, 112–122.

(33) Bruker AXS Inc. SADABS, APEX2; Bruker AXS Inc.: Madison, WI, 2014.

(34) Bruker AXS Inc. SAINT; Bruker AXS Inc.: Madison, WI, 2013.

(35) Sheldrick, G. M. SHELXT- Integrated space-group and crystal-structure determination. *Acta Crystallogr., Sect. A: Found. Crystallogr.* **2015**, *71*, 3–8.

(36) Sheldrick, G. M. Phase annealing in SHELX-90: direct methods for larger structures. *Acta Crystallogr., Sect. A: Found. Crystallogr.* **1990**, *46*, 467–473.

(37) Sheldrick, G. M. SHELXTL, version 6.10; Bruker AXS Inc.: Madison, WI, 2000.

(38) XP; Bruker AXS Inc.: Madison, WI, USA, 2014.

(39) Wikler, M. A. *Performance Standards for Antimicrobial Susceptibility Testing: Seventeenth Informational Supplement*; Clinical and Laboratory Standards Institute (CLSI), 2007.

(40) Marques, M. B.; Brookings, E. S.; Moser, S. A.; Sonke, P. B.; Waites, K. B. Comparative *in vitro* antimicrobial susceptibilities of nosocomial isolates of *Acinetobacter baumannii* and synergistic activities of nine antimicrobial combinations. *Antimicrob. Agents Chemother.* **1997**, *41*, 881–885.

(41) Theophel, K.; Schacht, V. J.; Schlüter, M.; Schnell, S.; Stingu, C.-S.; Schaumann, R.; Bunge, M. The importance of growth kinetic

analysis in determining bacterial susceptibility against antibiotics and silver nanoparticles. *Front. Microbiol.* **2014**, *5*, 544.

(42) Irfan, M.; Alam, S.; Manzoor, N.; Abid, M. Effect of quinoline based 1,2,3-triazole and its structural analogues on growth and virulence attributes of *Candida albicans*. *PLoS One* **2017**, *12*, No. e0175710.

(43) Baker, P. J. Regulation of the magnitude of the antibody response to bacterial polysaccharide antigens by thymus-derived lymphocytes. *Infect. Immun.* **1990**, *58*, 3465–3468.

(44) Felton, M. D.; Kauffmam, G.; Prescott, B.; Ottinger, B. Studies on the mechanism of immunological paralysis induced in mice by pneumococcal polysaccharides. *J. Immunol.* **1955**, *74*, 17–26.

(45) O'Toole, G. A.; Kolter, R. Initiation of biofilm formation in *Pseudomonas fluorescens* WCS365 proceeds via multiple, convergent signalling pathways: a genetic analysis. *Mol. Microbiol.* **1998**, *28*, 449–461.

(46) Antoci, V., Jr.; Adams, C. S.; Parvizi, J.; Davidson, H. M.; Composto, R. J.; Freeman, T. A.; Wickstrom, E.; Ducheyne, P.; Jungkind, D.; Shapiro, I. M.; Hickok, N. J. The inhibition of *Staphylococcus epidermidis* biofilm formation by vancomycin-modified titanium alloy and implications for the treatment of periprosthetic infection. *Biomaterials* **2008**, *29*, 4684–4690.